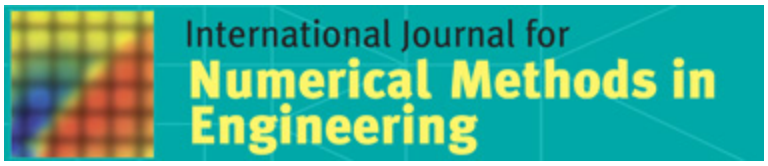

An artificial compressibility ensemble algorithm for a stochastic Stokes-Darcy model with random hydraulic conductivity and interface conditions

Journal:	*International Journal for Numerical Methods in Engineering*
Manuscript ID	NME-Apr-19-0226.R1
Wiley - Manuscript type:	Research Article
Date Submitted by the Author:	26-Aug-2019
Complete List of Authors:	He, Xiaoming; Missouri University of Science and Technology, Department of Mathematics and Statistics Jiang, Nan; Missouri University of Science and Technology, Department of Mathematics and Statistics Qiu, Changxin; Missouri University of Science and Technology
Keywords:	Ensemble method, Finite element methods, Artificial compressibility, Stokes-Darcy model, Random hydraulic conductivity, Interface conditions

Received: Added at production | Revised: Added at production | Accepted: Added at production

DOI: xxx/xxxx

RESEARCH ARTICLE

An artificial compressibility ensemble algorithm for a stochastic Stokes-Darcy model with random hydraulic conductivity and interface conditions

Xiaoming He[1] | Nan Jiang[1] | Changxin Qiu*[2]

[1]Department of Mathematics and Statistics, Missouri University of Science and Technology, Rolla, MO, 65409, USA
[2]Department of Mathematics, Iowa State University, Ames, IA, 50011, USA

Correspondence
*Changxin Qiu, Department of Mathematics, Iowa State University, Ames, IA, 50011, USA. Email: cxqiu@iastate.edu

Funding Information
This research was supported by the US National Science Foundation grants DMS-1722647, DMS-1720001.

Summary

We propose and analyze an efficient ensemble algorithm with artificial compressibility for fast decoupled computation of multiple realizations of the stochastic Stokes-Darcy model with random hydraulic conductivity (including the one in the interface conditions), source terms, and initial conditions. The solutions are found by solving three smaller decoupled subproblems with two common time-independent coefficient matrices for all realizations, which significantly improves the efficiency for both assembling and solving the matrix systems. The fully coupled Stokes-Darcy system can be first decoupled into two smaller sub-physics problems by the idea of the partitioned time stepping, which reduces the size of the linear systems and allows parallel computing for each sub-physics problem. The artificial compressibility further decouples the velocity and pressure which further reduces storage requirements and improves computational efficiency. We prove the long time stability and the convergence for this new ensemble method. Three numerical examples are presented to support the theoretical results and illustrate the features of the algorithm, including the convergence, stability, efficiency and applicability.

KEYWORDS:
Ensemble method, Artificial compressibility, Stokes-Darcy model, Random hydraulic conductivity, Interface conditions

1 | INTRODUCTION

There exist many interesting real world problems that involve a free flow and a porous medium flow[1,2,3,4,5,6,7,8], which can be described by the so called Stokes-Darcy type models. For example, in a karst aquifer, the flow in the conduits is governed by the Stokes equation and the porous media flow in the rock or soil is governed by the Darcy's law while these two flows are coupled on the interface between the conduits and the rock/soil[9,10,11]. In the Stokes-Darcy model, the Stokes equations describe the incompressible surface fluid flow and the Darcy equation describes the groundwater flow in porous media. Then these two equations are coupled by three interface conditions. More details and applications for this model can be found in[12,13,14,15,16,17,18,19,20,21,22,23,24,25,26,27,28,29]. Let D_f denote the surface fluid flow region and D_p the porous media flow region. Assume $D_f, D_p \subset R^d (d = 2, 3)$ are both open, bounded domains such that $D_f \cap D_p = \emptyset, \bar{D}_f \cap \bar{D}_p = I$, where I denotes the

interface between the two regions, see Figure 1. The traditional Stokes-Darcy model is recalled as follows,

$$\begin{aligned} u_t - \nu\Delta u + \nabla p = f_f(x,t), \nabla\cdot u = 0, \ \text{ in } \ D_f, \\ S_0\phi_t - \nabla\cdot(\mathcal{K}(x)\nabla\phi) = f_p(x,t), \ \text{ in } \ D_p, \\ \phi(x,0) = \phi_0(x), \ \text{in } D_p \text{ and } u(x,0) = u_0(x), \ \text{in } D_f, \\ \phi(x,t) = 0, \ \text{in } \partial D_p\backslash I \text{ and } u(x,t) = 0, \ \text{in } \partial D_f\backslash I. \end{aligned} \tag{1}$$

Let $\hat{n}_{f/p}$ denote the outward unit normal vector on I associated with $D_{f/p}$, where $\hat{n}_f = -\hat{n}_p$. The coupling conditions across I are conservation of mass, balance of forces and the Beavers-Joseph-Saffman condition on the tangential velocity:

$$\begin{aligned} u\cdot\hat{n}_f - \mathcal{K}\nabla\phi\cdot\hat{n}_p = 0 \text{ and } p - \nu\,\hat{n}_f\cdot\nabla u\cdot\hat{n}_f = g\phi \text{ on } I, \\ -\nu\,\nabla u\cdot\hat{n}_f = \frac{\alpha_{\mathrm{BJS}}}{\sqrt{\hat{\tau}_i\cdot\mathcal{K}\hat{\tau}_i}} u\cdot\hat{\tau}_i \ \text{ on } I, \ \text{for any tangential vector } \hat{\tau}_i \text{ on } I, \end{aligned}$$

see [30,31,32]. Here, g, $\mathcal{K}$, ν and S_0 are the gravitational acceleration constant, hydraulic conductivity tensor, kinematic viscosity and specific mass storativity coefficient, respectively, which are all positive. $\mathcal{K}$ is assumed to be symmetric positive definite (SPD).

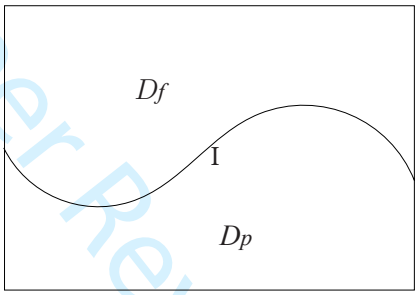

FIGURE 1 A sketch of the porous median domain D_p, fluid domain D_f, and the interface I.

For geophysical flows, accurate simulations are usually not feasible because of the difficult or impossible measurements of exact parameters in the physical world, e.g., the hydraulic conductivity tensor in the Stokes-Darcy model. Dealing with these uncertainties in the simulation usually involves first generating a set of samples in the stochastic parameter space described by an underlying random field with an prescribed covariance structure, which is usually determined by experiments, and then repeating simulations with different samples. As a result, the excessive computational cost in the process will be the main difficulty. Extensive efforts have been devoted to developing efficient UQ methods to overcome this challenge, among which the stochastic Galerkin [33,34], stochastic collocation [35,36,37,38] and polynomial chaos [39,40] are the most popular methods. In particular, non-intrusive methods, such as various variants of the Monte Carlo method [41,42], Latin hypercube sampling [43], centroidal Voronoi tessellations [44], stochastic collocation methods [35,36,37,38] and non-intrusive polynomial chaos methods [39,40], reuse existing PDE solvers/legacy codes to generate an ensemble of deterministic solutions which are used to approximate stochastic moments, are of high interest for feasibility and good parallel scalability on parallel computers. This line of research has been focused on reducing the amount of required simulation runs. Recently, another line of research has been initiated in [45] and has been receiving increasing attention. In [45], an ensemble algorithm was designed to solve all realizations simultaneously instead of solving them separately. It results in a common coefficient matrix for all realizations at each time step, which allows the use of efficient block solvers, e.g, block GMRES [46], block CG [47], or direct solvers such as LU factorization, to reduce both storage and computing time significantly. Some recent work on the ensemble algorithm include studying numerical regularizations for high Reynolds number flows [48,49], developing ensemble-based turbulence models [50], incorporating model reduction techniques to further reduce computational cost [51,52] and devising ensemble algorithms to account for uncertain model parameters for various flow equations [53,54,55,56,57,58,59]. As for the Stokes-Darcy system, the first study on efficient ensemble algorithms can be found in [60]. The ensemble algorithm can be incorporated with all the aforementioned non-intrusive UQ methods to further reduce the computational cost and potentially improve the performance of the overall stochastic simulations as the ensemble algorithm makes more simulations runs possible given a limited computation capacity.

The artificial compressibility (AC) methods were first studied in the 1960s to decouple the velocity and pressure by a regularization of the divergence-free constraint for incompressible fluid flow equations. The idea is to add a small perturbation, e.g.,

ϵp or ϵp_t, to the mass conservation equation and then eliminate the pressure from the momentum equation, so that one avoids 1) solving a saddle point problem at each time step, and 2) spurious boundary layers for the pressure caused by imposing artificial boundary conditions. Some of the first AC methods in the literature were proposed by Chorin[61], Temam[62,63,64], Vladimirova, Kuznetsov and Yanenko[65]. The AC methods can have severe time step restrictions if not discretized carefully,[61]. In a recent work, Guermond and Minev introduced a bootstraping technique to design unconditionally stable, higher order AC methods in[66]. The proposed methods, unlike the popular projection methods, which cannot exceed second-order accuracy in time without losing unconditional stability, can reach any order in time while being unconditionally stable (for the unsteady Stokes equations). DeCaria, Layton and McLaughlin[67] studied an unconditionally stable AC method based on a Crank-Nicolson Leapfrog time discretization for the Navier-Stokes equations. In[68], the artificial compressibility splitting method, which is extended from the penalty-projection method for the unsteady Navier-Stokes equations, was viewed as an hybrid two-step prediction-correction method by combining artificial compressibility method and an augmented Lagrangian method without inner iteration. Error analysis of some variants of AC method for computing the solutions of the Navier-Stokes problems can be found in[69,70]. Compared with the extensively studied Stokes/Navier-Stokes equations, the coupled time-dependent Stokes-Darcy equation is still in need of continued efforts for efficient methods in this area.

Based on the key ideas of[45,60] which was a fundamental development of the efficient ensemble algorithm for flow equations, in this article we utilize the idea of artificial compressibility and partitioned time stepping methods to construct the decoupled ensemble algorithm for efficiently computing multiple realizations of the stochastic Stokes-Darcy interface model with a random hydraulic conductivity tensor, source terms and initial conditions. In this algorithm, the originally coupled multi-physics model is decoupled by a two-level technique. The first level is to decouple the Stokes flow from the Darcy flow by the physical interface conditions and the partitioned time stepping method. The second level is to decouple the velocity and pressure by the artificial compressibility method in the Stokes equation. Hence, the Stokes-Darcy model is decoupled into three subproblems. One of the three subproblems is a straightforward update for the pressure. For each of the other two subproblems, all the realizations share the same coefficient matrix which is independent of time. The common coefficient matrix feature eliminates many redundant matrix operations, such as matrix assembly and matrix preprocess before solving the system. For example, if LU factorization is used to solve the linear systems, it only needs to be done once since every realization is sharing the same coefficient matrix, while a non-ensemble method would need to have, for example, 1000 matrices factorized. Hence the efficiency can be increased by a significant amount, which will be further explained in more details in the second numerical experiment. These features of the proposed algorithm significantly reduce the storage requirements and computational costs. Furthermore, compared with the previous works on non-interface problems in this area, extra efforts are required in order to deal with the randomness in the interface conditions of Stokes-Darcy system.

In this paper, we propose and study an artificial compressibility ensemble algorithm for computing an ensemble of the Stokes-Darcy systems to account for uncertainties in the hydraulic conductivity $\mathcal{K}(x)$, forcing terms $f_f(x,t)$, $f_p(x,t)$, and initial conditions $u^0(x), \phi^0(x)$. Herein we consider computing an ensemble of J Stokes-Darcy systems corresponding to J different parameter sets $(u_j^0, \phi_j^0, f_{fj}, f_{pj}, \mathcal{K}_j)$, $j = 1, ..., J$,

$$\begin{aligned} u_{j,t} - \nu_j \Delta u_j + \nabla p_j &= f_{f,j}(x,t),\ \nabla \cdot u_j = 0,\ \text{in } D_f, \\ S_0 \phi_{j,t} - \nabla \cdot \left(\mathcal{K}_j(x) \nabla \phi_j\right) &= f_{p,j}(x,t),\ \text{in } D_p, \\ \phi_j(x,t) = 0,\ \text{in } \partial D_p \backslash I \text{ and } u_j(x,t) &= 0,\ \text{in } \partial D_f \backslash I. \end{aligned} \tag{2}$$

The proposed algorithm (introduced in the Section 2) decouples the Stokes-Darcy model into three subproblems, two for the Stokes equation and one for the Darcy equation. Moreover, for the first and third subproblem, all realizations share the same common matrix at each time step, which allows the use of efficient block solvers, e.g, block CG[47], block GMRES[46], or direct solvers such as LU factorization, to reduce both storage and computation time. Based on the idea of artificial compressibility, the computation of pressure is decoupled from that of velocity. Hence, one can simply update the pressure at each time step without solving a Poisson problem, and no artificial boundary conditions are needed for the computation of the pressure which avoids the boundary layers for pressure errors.

This paper is organized into six sections. In Section 2 we establish the mathematical preliminaries and notations. In Section 3 we prove the long time stability of the proposed method under a time-step condition and two parameter conditions. In Section 3, an alternative approach for the case that $\mathcal{K}$ has simpler structures is proposed. We also prove the long time stability for this method under a similar time-step condition *without* any parameter conditions (see Appendix). The convergence and error

estimates for the proposed method are presented in Section 4. In Section 5, we present three numerical experiments to test the proposed ensemble method and our theoretical results. Finally, we make conclusions in Section 6.

2 | NOTATION AND PRELIMINARIES

We denote the $L^2(I)$ norm by $\|\cdot\|_I$ and the $L^2(D_{f/p})$ norms by $\|\cdot\|_{f/p}$; the corresponding inner products are denoted by $(\cdot,\cdot)_{f/p}$. Further, we denote the $H^k(D_{f/p})$ norm by $\|\cdot\|_{H^k(D_{f/p})}$. The following inequalities will be used in the proofs, [8].

$$\|\phi\|_I \le C(D_p)\sqrt{\|\phi\|_p\|\nabla\phi\|_p}, \tag{3}$$

$$\|u\|_I \le C(D_f)\sqrt{\|u\|_f\|\nabla u\|_f}, \tag{4}$$

where $C(D_{f/p}) = \mathcal{O}(\sqrt{L_{f/p}})$, $L_{f/p} = diameter(D_{f/p})$.

Define the function spaces:

$$\begin{aligned} \text{Velocity}: \quad & X_f := \{v \in \left(H^1(D_f)\right)^d : v = 0 \text{ on } \partial D_f \backslash I\}, \\ \text{Pressure}: \quad & Q_f := L^2(D_f), \\ \text{Hydraulic Head}: \quad & X_p := \{\psi \in H^1(D_p) : \psi = 0 \text{ on } \partial D_p \backslash I\}. \end{aligned}$$

For functions $v(x,t)$ defined on $(0,T)$, we define the continuous norm

$$\|v\|_{m,k,r} := \|v\|_{L^m(0,T;H^k(D_r))},\ r \in \{f,p\}.$$

Define

$$c_I(u,\phi) = g\int_I \phi u\cdot\hat{n}_f\, ds.$$

Let $C_{P,f}$ and $C_{P,p}$ be the Poincaré constants of the indicated domains and $\bar{k}_{min}(x)$ be the minimum eigenvalue of the mean hydraulic conductivity tensor $\bar{\mathcal{K}}(x)$. Define $\bar{k}_{min} = \min_{x\in\Omega_p}\bar{k}_{min}(x)$ and two parameter-dependent constants

$$C_1 = \frac{C_{P,f}^2[gC(D_f)C(D_p)]^4}{4\nu^2}, \qquad C_2 = \frac{C_{P,p}^2 g^2[C(D_f)C(D_p)]^4}{4\bar{k}_{min}^2}.$$

Then we have the following estimates for the coupling term $c_I(u,\phi)$.

Lemma 1. For any $(u,\phi)\in X_f\times X_p$ and any $\epsilon_1,\epsilon_2,\alpha_1,\beta_1>0$,

$$|c_I(u,\phi)| \le \frac{1}{4\epsilon_1}\|\phi\|_p^2 + \frac{\epsilon_1}{\alpha_1^2}C_1\|\nabla\phi\|_p^2 + \alpha_1\nu\|\nabla u\|_f^2, \tag{5}$$

$$|c_I(u,\phi)| \le \frac{1}{4\epsilon_2}\|u\|_f^2 + \frac{\epsilon_2}{\beta_1^2}C_2\|\nabla u\|_f^2 + \beta_1 g\bar{k}_{min}\|\nabla\phi\|_p^2. \tag{6}$$

Proof. See page 4 of [60]. □

The artificial compressibility ensemble algorithm we propose reads

Algorithm 1. Find $(u_j^{n+1}, p_j^{n+1}, \phi_j^{n+1})\in X_f\times Q_f\times X_p$ satisfying $\forall\,(v,\psi)\in X_f\times X_p$,

$$\begin{cases} \left(\dfrac{u_j^{n+1}-u_j^n}{\Delta t}, v\right)_f + \nu(\nabla u_j^{n+1},\nabla v)_f + \displaystyle\sum_i\int_I \bar{\eta}_i(u_j^{n+1}\cdot\hat{\tau}_i)(v\cdot\hat{\tau}_i)\,ds \\ + \displaystyle\sum_i\int_I(\eta_{i,j}-\bar{\eta}_i)(u_j^n\cdot\hat{\tau}_i)(v\cdot\hat{\tau}_i)\,ds + \gamma(\nabla\cdot u_j^{n+1},\nabla\cdot v)_f - \left(p_j^n,\nabla\cdot v\right)_f \\ + c_I(v,\phi_j^n) = (f_{f,j}^{n+1},v)_f, \end{cases} \quad \text{(sub-problem 1)}$$

$$p_j^{n+1} = p_j^n - \gamma\nabla\cdot u_j^{n+1}, \quad \text{(sub-problem 2)}$$

$$\begin{cases} gS_0\left(\dfrac{\phi_j^{n+1}-\phi_j^n}{\Delta t},\psi\right)_p + g(\bar{\mathcal{K}}\nabla\phi_j^{n+1},\nabla\psi)_p + g((\mathcal{K}_j-\bar{\mathcal{K}})\nabla\phi_j^n,\nabla\psi)_p \\ \qquad - c_I(u_j^n,\psi) = g(f_{p,j}^{n+1},\psi)_p, \end{cases} \quad \text{(sub-problem 3)}$$

where

$$\bar{\mathcal{K}} = \frac{1}{J}\sum_{j=1}^{J}\mathcal{K}_j, \quad \eta_{i,j} = \frac{\alpha_{\mathrm{BJS}}}{\sqrt{\widehat{\tau}_i\cdot\mathcal{K}_j\widehat{\tau}_i}} \quad \text{and} \quad \bar{\eta}_i = \frac{1}{J}\sum_{j=1}^{J}\eta_{i,j}.$$

Sub-problem 2 can be rewritten as $\frac{\Delta t}{\gamma}\frac{p_j^{n+1}-p_j^n}{\Delta t} + \nabla\cdot u_j^{n+1} = 0$. So γ should chosen to be $\mathcal{O}(1)$ or larger for the method to be first order convergent. Moving all the known quantities to the right hand side, the algorithm is as follows.

$$\begin{cases} \left(\dfrac{u_j^{n+1}-u_j^n}{\Delta t},v\right)_f + \nu(\nabla u_j^{n+1},\nabla v)_f + \displaystyle\sum_i\int_I \bar{\eta}_i(u_j^{n+1}\cdot\widehat{\tau}_i)(v\cdot\widehat{\tau}_i)\,ds \\ +\gamma(\nabla\cdot u_j^{n+1},\nabla\cdot v)_f = \left(p_j^n,\nabla\cdot v\right)_f + (f_{f,j}^{n+1},v)_f \\ -\displaystyle\sum_i\int_I(\eta_{i,j}-\bar{\eta}_i)(u_j^n\cdot\widehat{\tau}_i)(v\cdot\widehat{\tau}_i)\,ds - c_I(v,\phi_j^n), \end{cases} \quad \text{(sub-problem 1)}$$

$$p_j^{n+1} = p_j^n - \gamma\nabla\cdot u_j^{n+1}, \quad \text{(sub-problem 2)}$$

$$\begin{cases} gS_0\left(\dfrac{\phi_j^{n+1}-\phi_j^n}{\Delta t},\psi_h\right)_p + g(\bar{\mathcal{K}}\nabla\phi_j^{n+1},\nabla\psi)_p \\ \qquad = g(f_{p,j}^{n+1},\psi)_p - g((\mathcal{K}_j-\bar{\mathcal{K}})\nabla\phi_j^n,\nabla\psi)_p + c_I(u^n,\psi). \end{cases} \quad \text{(sub-problem 3)}$$

Remark 1. From the above algorithm, it is easy to see that the original coupled system is decoupled into three sub-problems i.e., the (sub-problem 1), (sub-problem 2) and (sub-problem 3) by the two-level technique. For all time steps and realizations, (sub-problem 1) can be solved by the linear systems with one common coefficient matrix since the coefficients of the unknowns are independent of both time and the ensemble index. The coefficients of the unknown interface term are always consistent at every time step because of the commonly used mean $\bar{\eta}_i$. Similarly, all realizations in (sub-problem 3) also share the common coefficient matrix for solving the linear systems. (sub-problems 2) is a straightforward update, which does not require solving any linear systems.

3 | STABILITY ANALYSIS

Let $|\cdot|_2$ denote the 2-norm of either vectors or matrices. Let $k_{j,min}(x)$, $\bar{k}_{min}(x)$ be the minimum eigenvalue of the hydraulic conductivity tensor $\mathcal{K}_j(x)$, $\bar{\mathcal{K}}(x)$ respectively, and $\rho_j'(x)$ be the spectral radius of the fluctuation of hydraulic conductivity tensor $\mathcal{K}_j(x)-\bar{\mathcal{K}}(x)$. Since both $\mathcal{K}_j(x)$ and $\bar{\mathcal{K}}(x)$ are symmetric, $|\mathcal{K}_j(x)-\bar{\mathcal{K}}(x)|_2 = \rho_j'(x)$. We then define the following quantities that will be used in our proof.

$$\eta_{i,j}'^{max} = \max_{x\in I}\left|\eta_{i,j}(x)-\bar{\eta}_i(x)\right|, \qquad \eta_i'^{max} = \max_j \eta_{i,j}'^{max}, \qquad \bar{\eta}_i^{min} = \min_{x\in I}\bar{\eta}_i(x),$$
$$k_{j,min} = \min_{x\in D_p} k_{j,min}(x), \qquad k_{min} = \min_j k_{j,min}, \qquad \bar{k}_{min} = \min_{x\in D_p}\bar{k}_{min}(x),$$
$$\rho_{j,max}' = \max_{x\in D_p}\rho_{j,max}'(x), \qquad \rho_{max}' = \max_j \rho_{j,max}'.$$

We prove the long time stability of Algorithm 1 under a time-step condition and two parameter conditions

$$\Delta t \le \min\left\{\frac{(1-\alpha_1-\alpha_2)\beta_1^2\bar{k}_{min}}{C_{P,p}^2}, \frac{(1-\beta_1-\beta_2-\frac{\rho'_{max}}{\bar{k}_{min}})\alpha_1^2 S_0\nu}{C_{P,f}^2}\right\}\frac{2\nu\bar{k}_{min}}{g^2[C(D_f)C(D_p)]^4}, \tag{7}$$

$$\eta_i'^{max} \le \bar{\eta}_i^{min}, \qquad \text{and} \qquad \rho'_{max} < \bar{k}_{min}. \tag{8}$$

Theorem 1 (Long time stability of Algorithm 1)**.** If the two parameter conditions in (8) both hold, and there exist $\alpha_1, \alpha_2, \beta_1, \beta_2$ in $(0, 1)$ such that the time-step condition (7) also holds, then Algorithm 1 is long time stable: for any $N > 0$,

$$\begin{aligned}
&\frac{1}{2}\|u_j^N\|_f^2 + \frac{gS_0}{2}\|\phi_j^N\|_p^2 + \Delta t^2\frac{C_2}{\beta_1^2}\|\nabla u_j^N\|_f^2 + \frac{\Delta t}{2\gamma}\|p_j^N\|_f^2 + \Delta t\sum_i\frac{\bar{\eta}_i^{min}}{2}\int_I (u_j^N\cdot\hat{\tau}_i)^2\,ds\\
&+\left(\Delta t^2\frac{1}{gS_0}\frac{C_1}{\alpha_1^2} + \Delta t\frac{g\rho'_{max}}{2}\right)\|\nabla\phi_j^N\|_p^2 + \frac{\Delta t}{2\gamma}\sum_{n=0}^{N-1}\|p_j^{n+1}-p_j^n\|_f^2\\
&\le \frac{1}{2}\|u_j^0\|_f^2 + \frac{gS_0}{2}\|\phi_j^0\|_p^2 + \Delta t^2\frac{C_2}{\beta_1^2}\|\nabla u_j^0\|_f^2 + \frac{\Delta t}{2\gamma}\|p_j^0\|_f^2 + \Delta t\sum_i\frac{\bar{\eta}_i^{min}}{2}\int_I (u_j^0\cdot\hat{\tau}_i)^2\,ds\\
&+\left(\Delta t^2\frac{1}{gS_0}\frac{C_1}{\alpha_1^2} + \Delta t\frac{g\rho'_{max}}{2}\right)\|\nabla\phi_j^0\|_p^2 + \Delta t\sum_{n=0}^{N-1}\frac{C_{P,f}^2}{4\alpha_2\nu}\|f_{f,j}^{n+1}\|_f^2 + \Delta t\sum_{n=0}^{N-1}\frac{gC_{P,p}^2}{4\beta_2\bar{k}_{min}}\|f_{p,j}^{n+1}\|_p^2.
\end{aligned} \tag{9}$$

Proof. Setting $v = u_j^{n+1}$, $\psi = \phi_j^{n+1}$ in Algorithm 1, replacing $\gamma\nabla\cdot u_j^{n+1}$ in the momentum equation by $p_j^{n+1} - p_j^n$, taking inner product of the mass conservation equation by $\gamma^{-1}p_j^{n+1}$, using $a^2 - ab = 1/2[a^2 - b^2 + (a-b)^2]$ and adding all three equations yields

$$\begin{aligned}
&\frac{1}{2\Delta t}\|u_j^{n+1}\|_f^2 - \frac{1}{2\Delta t}\|u_j^n\|_f^2 + \frac{1}{2\Delta t}\|u_j^{n+1}-u_j^n\|_f^2 + \nu\|\nabla u_j^{n+1}\|_f^2 + \sum_i\int_I\bar{\eta}_i(u_j^{n+1}\cdot\hat{\tau}_i)(u_j^{n+1}\cdot\hat{\tau}_i)\,ds\\
&+\frac{1}{2\gamma}\left(\|p_j^{n+1}\|_f^2 - \|p_j^n\|_f^2 + \|p_j^{n+1}-p_j^n\|_f^2\right) + \frac{gS_0}{2\Delta t}\|\phi_j^{n+1}\|_p^2 - \frac{gS_0}{2\Delta t}\|\phi_j^n\|_p^2 + \frac{gS_0}{2\Delta t}\|\phi_j^{n+1}-\phi_j^n\|_p^2\\
&+g(\bar{\mathcal{K}}\nabla\phi_j^{n+1},\nabla\phi_j^{n+1})_p + c_I(u_j^{n+1},\phi_j^n) - c_I(u_j^n,\phi_j^{n+1})\\
&=(f_{f,j}^{n+1},u_j^{n+1})_f + g(f_{p,j}^{n+1},\phi_j^{n+1})_p - \sum_i\int_I(\eta_{i,j}-\bar{\eta}_i)(u_j^n\cdot\hat{\tau}_i)(u_j^{n+1}\cdot\hat{\tau}_i)\,ds - g((\mathcal{K}_j-\bar{\mathcal{K}})\nabla\phi_j^n,\nabla\phi_j^{n+1})_p.
\end{aligned} \tag{10}$$

Applying estimates (5) and (6) with $\epsilon_1 = \frac{\Delta t}{2gS_0}$, $\epsilon_2 = \frac{\Delta t}{2}$, we have the same result as (3.7) in[60] as follows.

$$\begin{aligned}
&c_I(u_j^{n+1},\phi_j^n) - c_I(u_j^n,\phi_j^{n+1}) = c_I(u_j^{n+1}-u_j^n,\phi_j^{n+1}) - c_I(u_j^{n+1},\phi_j^{n+1}-\phi_j^n)\\
&\ge -\frac{1}{2\Delta t}\|u_j^{n+1}-u_j^n\|_f^2 - \Delta t\frac{C_2}{\beta_1^2}\left(\|\nabla u_j^{n+1}\|_f^2 + \|\nabla u_j^n\|_f^2\right) - \beta_1 g\bar{k}_{min}\|\nabla\phi_j^{n+1}\|_p^2\\
&\quad - \frac{gS_0}{2\Delta t}\|\phi_j^{n+1}-\phi_j^n\|_p^2 - \frac{\Delta t}{gS_0}\frac{C_1}{\alpha_1^2}\left(\|\nabla\phi_j^{n+1}\|_p^2 + \|\nabla\phi_j^n\|_p^2\right) - \alpha_1\nu\|\nabla u_j^{n+1}\|_f^2.
\end{aligned} \tag{11}$$

By using the Cauchy-Schwarz inequalities and Young's inequalities, for any $\alpha_2 > 0, \beta_2 > 0$ we have

$$\begin{aligned}
&(f_{f,j}^{n+1},u_j^{n+1})_f + g(f_{p,j}^{n+1},\phi_j^{n+1})_p\\
&\le \frac{C_{P,f}^2}{4\alpha_2\nu}\|f_{f,j}^{n+1}\|_f^2 + \alpha_2\nu\|\nabla u_j^{n+1}\|_f^2 + \frac{gC_{P,p}^2}{4\beta_2\bar{k}_{min}}\|f_{p,j}^{n+1}\|_p^2 + \beta_2 g\bar{k}_{min}\|\nabla\phi_j^{n+1}\|_p^2.
\end{aligned} \tag{12}$$

By recalling (3.9) in[60], the other two terms on the right hand side of (10) can be bounded as follows

$$\begin{aligned}
&-\sum_i\int_I(\eta_{i,j}-\bar{\eta}_i)(u_j^n\cdot\hat{\tau}_i)(u_j^{n+1}\cdot\hat{\tau}_i)\,ds\\
&\le\sum_i\left[\frac{\eta_i'^{max}}{2}\int_I(u_j^n\cdot\hat{\tau}_i)^2\,ds + \frac{\eta_i'^{max}}{2}\int_I(u_j^{n+1}\cdot\hat{\tau}_i)^2\,ds\right],
\end{aligned} \tag{13}$$

and

$$-g\left((\mathcal{K}_j-\bar{\mathcal{K}})\nabla\phi_j^n,\nabla\phi_j^{n+1}\right)_p \le g\int_{D_p}|\nabla\phi_j^{n+1}|_2|\mathcal{K}_j-\bar{\mathcal{K}}|_2|\nabla\phi_j^n|_2\,dx \le \frac{g\rho'_{max}}{2}\|\nabla\phi_j^n\|_p^2+\frac{g\rho'_{max}}{2}\|\nabla\phi_j^{n+1}\|_p^2. \tag{14}$$

Using above estimates, equation (10) becomes

$$\begin{aligned}&\frac{1}{2\Delta t}\|u_j^{n+1}\|_f^2-\frac{1}{2\Delta t}\|u_j^n\|_f^2+\left(1-\alpha_1-\alpha_2-\Delta t\frac{2C_2}{\beta_1^2\nu}\right)\nu\|\nabla u_j^{n+1}\|_f^2+\Delta t\frac{C_2}{\beta_1^2}\left(\|\nabla u_j^{n+1}\|_f^2-\|\nabla u_j^n\|_f^2\right)\\&+\sum_i\left[\frac{\bar{\eta}_i^{min}}{2}-\frac{\eta_i'^{max}}{2}\right]\int_I(u_j^{n+1}\cdot\hat{\tau}_i)^2\,ds+\sum_i\frac{\bar{\eta}_i^{min}}{2}\left[\int_I(u_j^{n+1}\cdot\hat{\tau}_i)^2\,ds-\int_I(u_j^n\cdot\hat{\tau}_i)^2\,ds\right]\\&+\sum_i\left[\frac{\bar{\eta}_i^{min}}{2}-\frac{\eta_i'^{max}}{2}\right]\int_I(u_j^n\cdot\hat{\tau}_i)^2\,ds+\frac{1}{2\gamma}\left(\|p_j^{n+1}\|_f^2-\|p_j^n\|_f^2+\|p_j^{n+1}-p_j^n\|_f^2\right)\\&+\frac{gS_0}{2\Delta t}\|\phi_j^{n+1}\|_p^2-\frac{gS_0}{2\Delta t}\|\phi_j^n\|_p^2+(1-\beta_1-\beta_2-\Delta t\frac{1}{g^2S_0\bar{k}_{min}}\frac{2C_1}{\alpha_1^2}-\frac{\rho'_{max}}{\bar{k}_{min}})g\bar{k}_{min}\|\nabla\phi_j^{n+1}\|_p^2\\&+\left(\Delta t\frac{1}{gS_0}\frac{C_1}{\alpha_1^2}+\frac{g\rho'_{max}}{2}\right)\left(\|\nabla\phi_j^{n+1}\|_p^2-\|\nabla\phi_j^n\|_p^2\right)\le\frac{C_{P,f}^2}{4\alpha_2\nu}\|f_{f,j}^{n+1}\|_f^2+\frac{gC_{P,p}^2}{4\beta_2\bar{k}_{min}}\|f_{p,j}^{n+1}\|_p^2.\end{aligned} \tag{15}$$

The stability holds if

$$1-\alpha_1-\alpha_2-\Delta t\frac{2C_2}{\beta_1^2\nu}\ge 0, \tag{16}$$

$$\frac{\bar{\eta}_i^{min}}{2}-\frac{\eta_i'^{max}}{2}\ge 0, \tag{17}$$

$$1-\beta_1-\beta_2-\Delta t\frac{1}{g^2S_0\bar{k}_{min}}\frac{2C_1}{\alpha_1^2}-\frac{\rho'_{max}}{\bar{k}_{min}}\ge 0. \tag{18}$$

Recall that $\alpha_1,\alpha_2,\beta_1,\beta_2,\Delta t,\eta_i'^{max},\rho'_{max}$ are all positive, we then have the following constraints on these parameters.

$$0<\alpha_1<1,\quad 0<\alpha_2<1,\qquad 0<\beta_1<1,\quad 0<\beta_2<1, \tag{19}$$

$$\frac{\rho'_{max}}{\bar{k}_{min}}<1,\quad \eta_i'^{max}\le\bar{\eta}_i^{min}, \tag{20}$$

$$\Delta t\le\min\left\{\frac{(1-\alpha_1-\alpha_2)\beta_1^2\nu}{2C_2},\frac{(1-\beta_1-\beta_2-\frac{\rho'_{max}}{\bar{k}_{min}})\alpha_1^2g^2S_0\bar{k}_{min}}{2C_1}\right\}. \tag{21}$$

(20) leads to the two parameter conditions in (8), and (21) leads to the time-step condition (7) required for stability. Now if the time-step condition (7) and the two parameter conditions in (8) all hold, (15) reduces to

$$\begin{aligned}&\frac{1}{2\Delta t}\|u_j^{n+1}\|_f^2-\frac{1}{2\Delta t}\|u_j^n\|_f^2+\Delta t\frac{C_2}{\beta_1^2}\left(\|\nabla u_j^{n+1}\|_f^2-\|\nabla u_j^n\|_f^2\right)\\&+\sum_i\frac{\bar{\eta}_i^{min}}{2}\left[\int_I(u_j^{n+1}\cdot\hat{\tau}_i)^2\,ds-\int_I(u_j^n\cdot\hat{\tau}_i)^2\,ds\right]+\frac{1}{2\gamma}\left(\|p_j^{n+1}\|_f^2-\|p_j^n\|_f^2+\|p_j^{n+1}-p_j^n\|_f^2\right)\\&+\frac{gS_0}{2\Delta t}\|\phi_j^{n+1}\|_p^2-\frac{gS_0}{2\Delta t}\|\phi_j^n\|_p^2+\left(\Delta t\frac{1}{gS_0}\frac{C_1}{\alpha_1^2}+\frac{g\rho'_{max}}{2}\right)\left(\|\nabla\phi_j^{n+1}\|_p^2-\|\nabla\phi_j^n\|_p^2\right)\\&\le\frac{C_{P,f}^2}{4\alpha_2\nu}\|f_{f,j}^{n+1}\|_f^2+\frac{gC_{P,p}^2}{4\beta_2\bar{k}_{min}}\|f_{p,j}^{n+1}\|_p^2.\end{aligned} \tag{22}$$

Sum (22) from $n = 0$ to $N-1$ and multiply it by Δt to get

$$\begin{aligned}
&\frac{1}{2}\|u_j^N\|_f^2 + \frac{gS_0}{2}\|\phi_j^N\|_p^2 + \Delta t^2\frac{C_2}{\beta_1^2}\|\nabla u_j^N\|_f^2 + \frac{\Delta t}{2\gamma}\|p_j^N\|_f^2 + \Delta t\sum_i \frac{\bar{\eta}_i^{min}}{2}\int_I (u_j^N\cdot\hat{\tau}_i)^2\,ds \\
&+\left(\Delta t^2\frac{1}{gS_0}\frac{C_1}{\alpha_1^2} + \Delta t\frac{g\rho'_{max}}{2}\right)\|\nabla\phi_j^N\|_p^2 + \frac{\Delta t}{2\gamma}\sum_{n=0}^{N-1}\|p_j^{n+1}-p_j^n\|_f^2 \\
&\le \frac{1}{2}\|u_j^0\|_f^2 + \frac{gS_0}{2}\|\phi_j^0\|_p^2 + \Delta t^2\frac{C_2}{\beta_1^2}\|\nabla u_j^0\|_f^2 + \frac{\Delta t}{2\gamma}\|p_j^0\|_f^2 + \Delta t\sum_i \frac{\bar{\eta}_i^{min}}{2}\int_I (u_j^0\cdot\hat{\tau}_i)^2\,ds \\
&+\left(\Delta t^2\frac{1}{gS_0}\frac{C_1}{\alpha_1^2} + \Delta t\frac{g\rho'_{max}}{2}\right)\|\nabla\phi_j^0\|_p^2 + \Delta t\sum_{n=0}^{N-1}\frac{C_{P,f}^2}{4\alpha_2\nu}\|f_{f,j}^{n+1}\|_f^2 + \Delta t\sum_{n=0}^{N-1}\frac{gC_{P,p}^2}{4\beta_2\bar{k}_{min}}\|f_{p,j}^{n+1}\|_p^2,
\end{aligned} \tag{23}$$

which completes the proof. □

Remark 2. If $\mathcal{K}_j(x)$ is diagonal, an alternative artificial compressiblity ensemble algorithm can be devised to remove the parameter conditions for stability.

Algorithm 2. Find $(u_j^{n+1}, p_j^{n+1}, \phi_j^{n+1}) \in X_f \times Q_f \times X_p$ satisfying $\forall\,(v,\psi) \in X_f \times X_p$,

$$\begin{cases}
\left(\dfrac{u_j^{n+1}-u_j^n}{\Delta t}, v\right)_f + \nu(\nabla u_j^{n+1}, \nabla v)_f + \displaystyle\sum_i \int_I \eta_i^{max}(u_j^{n+1}\cdot\hat{\tau}_i)(v\cdot\hat{\tau}_i)\,ds \\
+\displaystyle\sum_i \int_I (\eta_{i,j}-\eta_i^{max})(u_j^n\cdot\hat{\tau}_i)(v\cdot\hat{\tau}_i)\,ds + \gamma(\nabla\cdot u_j^{n+1}, \nabla\cdot v)_f - \left(p_j^n, \nabla\cdot v\right)_f \\
\qquad + c_I(v,\phi_j^n) = (f_{f,j}^{n+1}, v)_f,
\end{cases} \tag{sub-problem 1}$$

$$p_j^{n+1} = p_j^n - \gamma\nabla\cdot u_j^{n+1}, \tag{sub-problem 2}$$

$$\begin{cases}
gS_0\left(\dfrac{\phi_j^{n+1}-\phi_j^n}{\Delta t}, \psi_h\right)_p + k_{max}g(\nabla\phi_j^{n+1}, \nabla\psi)_p + g((\mathcal{K}_j - k_{max}\mathcal{I})\nabla\phi_j^n, \nabla\psi)_p \\
\qquad - c_I(u_j^n, \psi_h) = g(f_{p,j}^{n+1}, \psi)_p,
\end{cases} \tag{sub-problem 3}$$

where $k_{j,max}(x)$ is the maximum eigenvalue of the hydraulic conductivity tensor $\mathcal{K}_j(x)$, and

$$\eta_{i,j}^{max} = \max_{x\in I}\eta_{i,j}(x), \qquad \eta_i^{max} = \max_j \eta_{i,j}^{max}, \qquad k_{j,max} = \max_{x\in D_p} k_{j,max}(x), \qquad k_{max} = \max_j k_{j,max}.$$

We can prove long time stability of Algorithm 2 under a similar time-step condition, *without* any parameter conditions.

$$\Delta t \le \min\left\{\frac{(1-\alpha_1-\alpha_2)\beta_1^2 k_{max}}{C_{P,p}^2}, \frac{(1-\beta_1-\beta_2-\frac{k_{max}-k_{min}}{k_{max}})\alpha_1^2 S_0\nu}{C_{P,f}^2}\right\}\frac{2\nu k_{max}}{g^2[C(D_f)C(D_p)]^4}. \tag{24}$$

The proof is given in Appendix.

4 | ERROR ANALYSIS

In this section, we give a detailed error analysis for Algorithm 1. We assume the following regularity on the true solution of the Stokes-Darcy equations.

$$\begin{aligned}
&u_{j,t} \in L^2(0,T;H(D_f)), u_{j,tt} \in L^2(0,T;L^2(D_f)), \phi_{j,t} \in L^2(0,T;H^1(D_p)), \phi_{j,tt} \in L^2(0,T;L^2(D_p)), \\
&p_{j,t} \in L^\infty(0,T;L^2(D_f)), p_{j,tt} \in L^\infty(-T,T;L^2(D_f)).
\end{aligned}$$

Let $e^n_{j,u} := u_j(t_n) - u^n_j, e^n_{j,p} := p_j(t_n) - p^n_j, e^n_{j,\phi} := \phi_j(t_n) - \phi^n_{j,h}$ denote the errors at t_n between the true solution $(u_j(t_n), p_j(t_n), \phi_j(t_n))$ of (2) and the approximation (u^n_j, p^n_j, ϕ^n_j) obtained using the AC ensemble Algorithm 1. We prove the convergence of Algorithm 1 under a time-step condition and two parameter conditions.

$$\Delta t \le \min\left\{\frac{(1-\alpha_1-\alpha_2)\beta_1^2\bar{k}_{min}}{C^2_{P,p}}, \frac{(1-\beta_1-\beta_2-(1+\beta_3)\frac{\rho'_{max}}{\bar{k}_{min}})\alpha_1^2 S_0\nu}{C^2_{P,f}}\right\}\frac{2\nu\bar{k}_{min}}{g^2[C(D_f)C(D_p)]^4}, \tag{25}$$

$$\eta_i'^{max} \le \bar{\eta}_i^{min} \qquad \text{and} \qquad \rho'_{max} < \bar{k}_{min}. \tag{26}$$

Theorem 2 (Error Estimate)**.** For any $j = 1, \dots, J$, if the two parameter conditions in (26) hold, and there exist $\alpha_1, \alpha_2, \beta_1, \beta_2 \in (0,1)$ and $\beta_3 > 0$ such that the time-step condition (25) also holds, then there is a positive constant C independent of the time step Δt such that

$$\frac{1}{2}\|e^N_{j,u}\|^2_f + (\frac{\alpha_2}{3}\nu\Delta t + \Delta t^2\frac{C_2}{\beta_1^2})\|\nabla e^N_{j,u}\|^2_f + \sum_i(\sigma_2+\frac{1}{2})\Delta t\eta_i'^{max}\int_I (e^N_{j,u}\cdot\hat{\tau}_i)^2\,ds + \frac{gS_0}{2}\|e^N_{j,\phi}\|^2_p \tag{27}$$

$$+\left(\frac{\beta_2}{2}g\bar{k}_{min} + \frac{1}{2}g\rho'_{max} + \frac{\Delta t C_1}{gS_0\alpha_1^2}\right)\Delta t\|\nabla e^N_{j,\phi}\|^2_p + \frac{1}{2\gamma}\Delta t\|e^N_{j,p}\|^2_f + \sum_{n=0}^{N-1}\frac{1}{2\gamma}\Delta t\|e^{n+1}_{j,p} - e^n_{j,p}\|^2_f \le C\Delta t^2.$$

Proof. For $\forall v \in X_f, \forall\psi \in X_p, \forall q \in Q_f$, the true solution (u_j, p_j, ϕ_j) satisfies

$$\left(\frac{u_j(t_{n+1}) - u_j(t_n)}{\Delta t}, v\right)_f + \nu(\nabla u_j(t_{n+1}), \nabla v)_f + \sum_i\int_I \eta_{i,j}(u_j(t_{n+1})\cdot\hat{\tau}_i)(v\cdot\hat{\tau}_i)\,ds$$
$$-\left(p_j(t_{n+1}), \nabla\cdot v\right)_f + c_I(v, \phi_j(t_n)) = (f^{n+1}_{f,j}, v)_f + \epsilon^{n+1}_{j,f}(v), \tag{28}$$

$$\left(p_j(t_{n+1}) - p_j(t_n), q\right)_f + \gamma(\nabla\cdot u_j(t_{n+1}), q)_f = \left(p_j(t_{n+1}) - p_j(t_n), q\right)_f, \tag{29}$$

$$gS_0\left(\frac{\phi_j(t_{n+1}) - \phi_j(t_n)}{\Delta t}, \psi\right)_p + g(\mathcal{K}_j\nabla\phi_j(t_{n+1}), \nabla\psi_h)_p - c_I(u_j(t_n), \psi) = g(f^{n+1}_{p,j}, \psi)_p + \epsilon^{n+1}_{j,p}(\psi). \tag{30}$$

The consistency errors $\epsilon^{n+1}_{j,f}(v), \epsilon^{n+1}_{j,p}(\psi)$ are defined by

$$\epsilon^{n+1}_{j,f}(v) := \left(\frac{u_j(t_{n+1}) - u_j(t_n)}{\Delta t} - u_{j,t}(t_{n+1}), v\right)_f - c_I(v, \phi_j(t_{n+1}) - \phi_j(t_n)),$$
$$\epsilon^{n+1}_{j,p}(\psi) := gS_0\left(\frac{\phi_j(t_{n+1}) - \phi_j(t_n)}{\Delta t} - \phi_{j,t}(t_{n+1}), \psi\right)_p + c_I(u_j(t_{n+1}) - u_j(t_n), \psi).$$

Subtracting Algorithm 1 from (28)-(30), then for $\forall v \in X_f, \forall\psi \in X_p, \forall q \in Q_f$,

$$\left(\frac{e^{n+1}_{j,u} - e^n_{j,u}}{\Delta t}, v\right)_f + \nu(\nabla e^{n+1}_{j,u}, \nabla v)_f + \sum_i\int_I \bar{\eta}_i(e^{n+1}_{j,u}\cdot\hat{\tau}_i)(v\cdot\hat{\tau}_i)\,ds$$
$$+\sum_i\int_I\left(\eta_{i,j} - \bar{\eta}_i\right)(e^n_{j,u}\cdot\hat{\tau}_i)(v\cdot\hat{\tau}_i)\,ds - \left(e^{n+1}_{j,p}, \nabla\cdot v\right)_f + c_I(v, e^n_{j,\phi})$$
$$= -\sum_i\int_I\left(\eta_{i,j} - \bar{\eta}_i\right)((u^{n+1}_j - u^n_j)\cdot\hat{\tau}_i)(v\cdot\hat{\tau}_i)\,ds + \epsilon^{n+1}_{j,f}(v), \tag{31}$$

$$\frac{1}{\gamma}\left(e^{n+1}_{j,p} - e^n_{j,p}, q\right)_f + (\nabla\cdot e^{n+1}_{j,u}, q)_f = \frac{1}{\gamma}\left(p_j(t_{n+1}) - p_j(t_n), q\right)_f, \tag{32}$$

$$gS_0\left(\frac{e^{n+1}_{j,\phi} - e^n_{j,\phi}}{\Delta t}, \psi\right)_p + g(\bar{\mathcal{K}}\nabla e^{n+1}_{j,\phi}, \nabla\psi)_p + g((\mathcal{K}_j - \bar{\mathcal{K}})\nabla e^n_{j,\phi}, \nabla\psi)_p - c_I(e^n_{j,u}, \psi) \tag{33}$$
$$= -g((\mathcal{K}_j - \bar{\mathcal{K}})\nabla(\phi^{n+1}_j - \phi^n_j), \nabla\psi)_p + \epsilon^{n+1}_{j,p}(\psi).$$

Setting $v = e^{n+1}_{j,u}, q = e^{n+1}_{j,p}, \psi = e^{n+1}_{j,\phi}$ in (31) -(33) and adding the three equations yields

$$\frac{1}{2\Delta t}\|e_{j,u}^{n+1}\|_f^2 - \frac{1}{2\Delta t}\|e_{j,u}^{n}\|_f^2 + \frac{1}{2\Delta t}\|e_{j,u}^{n+1} - e_{j,u}^{n}\|_f^2 + \nu\|\nabla e_{j,u}^{n+1}\|_f^2 + \sum_i \int_I \bar{\eta}_i (e_{j,u}^{n+1}\cdot\hat{\tau}_i)^2\, ds$$
$$+ \frac{gS_0}{2\Delta t}\|e_{j,\phi}^{n+1}\|_p^2 - \frac{gS_0}{2\Delta t}\|e_{j,\phi}^{n}\|_p^2 + \frac{gS_0}{2\Delta t}\|e_{j,\phi}^{n+1} - e_{j,\phi}^{n}\|_p^2 + g(\bar{\mathcal{K}}\nabla e_{j,\phi}^{n+1}, \nabla e_{j,\phi}^{n+1})_p + c_I(e_{j,u}^{n+1}, e_{j,\phi}^{n})$$
$$- c_I(e_{j,u}^{n}, e_{j,\phi}^{n+1}) + \frac{1}{2\gamma}\left(\|e_{j,p}^{n+1}\|_f^2 - \|e_{j,p}^{n}\|^2\right) + \frac{1}{2\gamma}\|e_{j,p}^{n+1} - e_{j,p}^{n}\|_f^2 \tag{34}$$
$$= -\sum_i \int_I \left(\eta_{i,j} - \bar{\eta}_i\right)(e_{j,u}^{n}\cdot\hat{\tau}_i)(e_{j,u}^{n+1}\cdot\hat{\tau}_i)\, ds - \sum_i \int_I \left(\eta_{i,j} - \bar{\eta}_i\right)((u_j^{n+1} - u_j^{n})\cdot\hat{\tau}_i)(e_{j,u}^{n+1}\cdot\hat{\tau}_i)\, ds$$
$$+ \epsilon_{j,f}^{n+1}(e_{j,u}^{n+1}) + \frac{1}{\gamma}\left(p_j(t_{n+1}) - p_j(t_n), e_{j,p}^{n+1}\right)_f - g((\mathcal{K}_j - \bar{\mathcal{K}})\nabla(\phi_j^{n+1} - \phi_j^{n}), \nabla e_{j,\phi}^{n+1})_p$$
$$- g((\mathcal{K}_j - \bar{\mathcal{K}})\nabla e_{j,\phi}^{n}, \nabla e_{j,\phi}^{n+1})_p + \epsilon_{j,p}^{n+1}(e_{j,\phi}^{n+1}).$$

Using the same technique in the stability proof (see (11)), we have for any $\alpha_1, \beta_1 > 0$

$$c_I(e_{j,u}^{n+1}, e_{j,\phi}^{n}) - c_I(e_{j,u}^{n}, e_{j,\phi}^{n+1}) = c_I(e_{j,u}^{n+1} - e_{j,u}^{n}, e_{j,\phi}^{n+1}) - c_I(e_{j,u}^{n+1}, e_{j,\phi}^{n+1} - e_{j,\phi}^{n})$$
$$\geq -\frac{1}{2\Delta t}\|e_{j,u}^{n+1} - e_{j,u}^{n}\|_f^2 - \Delta t\frac{C_2}{\beta_1^2}\left(\|\nabla e_{j,u}^{n+1}\|_f^2 + \|\nabla e_{j,u}^{n}\|_f^2\right) - \beta_1 g\bar{k}_{min}\|\nabla e_{j,\phi}^{n+1}\|_p^2 \tag{35}$$
$$- \frac{gS_0}{2\Delta t}\|e_{j,\phi}^{n+1} - e_{j,\phi}^{n}\|_p^2 - \frac{\Delta t}{gS_0}\frac{C_1}{\alpha_1^2}\left(\|\nabla e_{j,\phi}^{n+1}\|_p^2 + \|\nabla e_{j,\phi}^{n}\|_p^2\right) - \alpha_1\nu\|\nabla e_{j,u}^{n+1}\|_f^2.$$

Next we bound the terms on the right hand side of (34) one by one. First,

$$-\sum_i \int_I \left(\eta_{i,j} - \bar{\eta}_i\right)(e_{j,u}^{n}\cdot\hat{\tau}_i)(e_{j,u}^{n+1}\cdot\hat{\tau}_i)\, ds \leq \sum_i \eta_{i,j}'^{max} \int_I |(e_{j,u}^{n}\cdot\hat{\tau}_i)(e_{j,u}^{n+1}\cdot\hat{\tau}_i)|\, ds$$
$$\leq \sum_i \left[\frac{\eta_i'^{max}}{2}\int_I (e_{j,u}^{n}\cdot\hat{\tau}_i)^2\, ds + \frac{\eta_i'^{max}}{2}\int_I (e_{j,u}^{n+1}\cdot\hat{\tau}_i)^2\, ds\right]. \tag{36}$$

By Poincaré inequality and (4), for any $\sigma_1 > 0$, we can get

$$-\sum_i \int_I \left(\eta_{i,j} - \bar{\eta}_i\right)((u_j^{n+1} - u_j^{n})\cdot\hat{\tau}_i)(e_{j,u}^{n+1}\cdot\hat{\tau}_i)\, ds \tag{37}$$
$$\leq \sum_i \left[\frac{C}{\sigma_1}\eta_i'^{max}\Delta t\int_{t_n}^{t_{n+1}} \|\nabla u_{j,t}\|_f^2\, dt + \sigma_1\eta_i'^{max}\int_I (e_{j,u}^{n+1}\cdot\hat{\tau}_i)^2\, ds\right].$$

Next we bound the consistency errors.

$$\epsilon_{j,f}^{n+1}(e_{j,u}^{n+1}) \leq C\left\|\frac{u_j(t_{n+1}) - u_j(t_n)}{\Delta t} - u_{j,t}(t_{n+1})\right\|_f^2 + C\|\nabla(\phi_j(t_{n+1}) - \phi_j(t_n))\|_p^2 + \alpha_2\nu\|\nabla e_{j,u}^{n+1}\|_f^2 \tag{38}$$
$$\leq C\Delta t\int_{t_n}^{t_{n+1}} \|u_{j,tt}(t)\|_f^2\, dt + C\Delta t\int_{t_n}^{t_{n+1}} \|\nabla\phi_{j,t}(t)\|_p^2\, dt + \frac{\alpha_2}{3}\nu\|\nabla e_{j,u}^{n+1}\|_f^2.$$

$$\epsilon_{j,p}^{n+1}(e_{j,\phi}^{n+1}) \leq C\left\|\frac{\phi_j(t_{n+1}) - \phi_j(t_n)}{\Delta t} - \phi_{j,t}(t_{n+1})\right\|_p^2 + C\|\nabla(u_j(t_{n+1}) - u_j(t_n))\|_f^2 + \beta_2 g\bar{k}_{min}\|\nabla e_{j,\phi}^{n+1}\|_p^2$$
$$\leq C\Delta t\int_{t_n}^{t_{n+1}} \|\phi_{j,tt}(t)\|_p^2\, dt + C\Delta t\int_{t_n}^{t_{n+1}} \|\nabla u_{j,t}(t)\|_f^2\, dt + \frac{\beta_2}{2}g\bar{k}_{min}\|\nabla e_{j,\phi}^{n+1}\|_p^2. \tag{39}$$

The hydraulic conductivity tensor terms are estimated as follows.

$$-g((\mathcal{K}_j - \bar{\mathcal{K}})\nabla e_{j,\phi}^{n}, \nabla e_{j,\phi}^{n+1})_p \leq \frac{g\rho'_{max}}{2}\|\nabla e_{j,\phi}^{n}\|_p^2 + \frac{g\rho'_{max}}{2}\|\nabla e_{j,\phi}^{n+1}\|_p^2. \tag{40}$$

For any $\beta_3 > 0$, we have

$$-g((\mathcal{K}_j - \bar{\mathcal{K}})\nabla(\phi_j^{n+1} - \phi_j^n), \nabla e_{j,\phi}^{n+1})_p \le \frac{Cg\rho'_{max}}{\beta_3}\Delta t \int_{t_n}^{t_{n+1}} \|\nabla\phi_{j,t}\|_p^2\, dt + \beta_3 g\rho'_{max}\|\nabla e_{j,\phi}^{n+1}\|_p^2. \tag{41}$$

Lastly, we bound the pressure term. Consider the decomposition $H_0^1(\Omega) = Y \oplus Y^\perp$, where $Y^\perp = \{(-\Delta)^{-1}\nabla q : q \in L^2(\Omega)\}$, see[71,69]. For $p_{j,t}(t), p_{j,tt}(t) \in L^2(\Omega)/\mathbb{R}$, there exists a unique $\mu_j(t)$ such that $\nabla\cdot\mu_j(t) = p_{j,t}(t)$, $\nabla\cdot\mu_{j,t}(t) = p_{j,tt}(t)$, and we have

$$\|\nabla\mu_j(t)\| \le C\|p_{j,t}(t)\|, \quad \|\nabla\mu_{j,t}(t)\| \le C\|p_{j,tt}(t)\|, \qquad \forall t \in [0,T].$$

We will use this result in the following estimates.

The pressure term can be rewritten using (31) as

$$\begin{aligned}
&\frac{1}{\gamma}\left(p_j(t_{n+1}) - p_j(t_n), e_{j,p}^{n+1}\right)_f = \frac{1}{\gamma}\left(\int_{t_n}^{t_{n+1}} p_{j,t}(t)\, dt, e_{j,p}^{n+1}\right)_f \\
&= \frac{1}{\gamma}\left(\int_{t_n}^{t_{n+1}} \nabla\cdot\mu_j(t)\, dt, e_{j,p}^{n+1}\right)_f = -\frac{1}{\gamma}\left(\int_{t_n}^{t_{n+1}} \mu_j(t)\, dt, \nabla e_{j,p}^{n+1}\right)_f \\
&= \frac{1}{\gamma}\left(\frac{e_{j,u}^{n+1} - e_{j,u}^n}{\Delta t}, \int_{t_n}^{t_{n+1}} \mu_j(t)\, dt\right)_f + \frac{\nu}{\gamma}(\nabla e_{j,u}^{n+1}, \int_{t_n}^{t_{n+1}} \nabla\mu_j(t)\, dt)_f \\
&\quad + \frac{1}{\gamma}\sum_i \int_I \bar{\eta}_i(e_{j,u}^{n+1}\cdot\hat{\tau}_i)(\int_{t_n}^{t_{n+1}} \mu_j(t)\, dt\cdot\hat{\tau}_i)\, ds + \frac{1}{\gamma}\sum_i \int_I \left(\eta_{i,j} - \bar{\eta}_i\right)(e_{j,u}^n\cdot\hat{\tau}_i)(\int_{t_n}^{t_{n+1}} \mu(t)\, dt\cdot\hat{\tau}_i)\, ds \\
&\quad + \frac{1}{\gamma}c_I(\int_{t_n}^{t_{n+1}} \mu_j(t)\, dt, e_{j,\phi}^n) + \frac{1}{\gamma}\sum_i \int_I \left(\eta_{i,j} - \bar{\eta}_i\right)((u_j(t_{n+1}) - u_j(t_n))\cdot\hat{\tau}_i)(\int_{t_n}^{t_{n+1}} \mu(t)\, dt\cdot\hat{\tau}_i)\, ds \\
&\quad - \frac{1}{\gamma}\epsilon_{j,f}^{n+1}(\int_{t_n}^{t_{n+1}} \mu_j(t)\, dt).
\end{aligned} \tag{42}$$

We need to bound each term on the right hand side of (42).

$$\begin{aligned}
&-\frac{1}{\gamma}\epsilon_{j,f}^{n+1}(\int_{t_n}^{t_{n+1}} \mu(t)\, dt) \\
&\le \frac{C}{\gamma}\left\|\frac{u_j(t_{n+1}) - u_j(t_n)}{\Delta t} - u_{j,t}(t_{n+1})\right\|_f^2 + \frac{C}{\gamma}\|\nabla(\phi_j(t_{n+1}) - \phi_j(t_n))\|_p^2 + \frac{C}{\gamma}\|\int_{t_n}^{t_{n+1}} \nabla\mu_j(t)\, dt\|_f^2 \\
&\le \frac{C}{\gamma}\Delta t \int_{t^n}^{t^{n+1}} \|u_{j,tt}(t)\|_f^2\, dt + \frac{C}{\gamma}\Delta t \int_{t^n}^{t^{n+1}} \|\nabla\phi_{j,t}(t)\|_p^2\, dt + \frac{C}{\gamma}\nu\Delta t \int_{t_n}^{t_{n+1}} \|\nabla\mu_j(t)\|_f^2 dt \\
&\le C\Delta t \int_{t^n}^{t^{n+1}} \|u_{j,tt}(t)\|_f^2\, dt + C\Delta t \int_{t^n}^{t^{n+1}} \|\nabla\phi_{j,t}(t)\|_p^2\, dt + \frac{C}{\gamma}\nu\Delta t \int_{t_n}^{t_{n+1}} \|p_{j,t}(t)\|_f^2 dt.
\end{aligned} \tag{43}$$

$$\frac{\nu}{\gamma}(\nabla e_{j,u}^{n+1}, \int_{t_n}^{t_{n+1}} \nabla\mu_j(t)\, dt)_f \le \frac{\alpha_2}{3}\nu\Delta t\|\nabla e_{j,u}^{n+1}\|_f^2 + \frac{C\nu\Delta t}{\alpha_2\gamma^2}\int_{t_n}^{t_{n+1}} \|p_{j,t}(t)\|_f^2 dt. \tag{44}$$

$$
\begin{aligned}
&\frac{1}{\gamma}\left(\frac{e_{j,u}^{n+1}-e_{j,u}^{n}}{\Delta t},\int_{t_n}^{t_{n+1}}\mu_j(t)\,dt\right)_f \\
&=\frac{1}{\gamma\Delta t}\left[\left(e_{j,u}^{n+1},\int_{t_n}^{t_{n+1}}\mu_j(t)\,dt\right)_f-\left(e_{j,u}^{n},\int_{t_{n-1}}^{t_n}\mu_j(t)\,dt\right)_f\right]-\frac{1}{\gamma\Delta t}\left(e_{j,u}^{n},\int_{t_n}^{t_{n+1}}\mu_j(t)\,dt-\int_{t_{n-1}}^{t_n}\mu_j(t)\,dt\right)_f \\
&\le\frac{1}{\gamma\Delta t}\left[\left(e_{j,u}^{n+1},\int_{t_n}^{t_{n+1}}\mu_j(t)\,dt\right)_f-\left(e_{j,u}^{n},\int_{t_{n-1}}^{t_n}\mu_j(t)\,dt\right)_f\right]+\frac{2\Delta t}{\gamma}\left|\left(e_{j,u}^{n},\mu_{j,t}(\xi_n)\right)_f\right| \\
&\le\frac{1}{\gamma\Delta t}\left[\left(e_{j,u}^{n+1},\int_{t_n}^{t_{n+1}}\mu_j(t)\,dt\right)_f-\left(e_{j,u}^{n},\int_{t_{n-1}}^{t_n}\mu_j(t)\,dt\right)_f\right]+\frac{2\Delta t}{\gamma}\|e_{j,u}^{n}\|_f\|\mu_{j,t}(\xi_n)\|_f \\
&\le\frac{1}{\gamma\Delta t}\left[\left(e_{j,u}^{n+1},\int_{t_n}^{t_{n+1}}\mu_j(t)\,dt\right)_f-\left(e_{j,u}^{n},\int_{t_{n-1}}^{t_n}\mu_j(t)\,dt\right)_f\right]+\frac{\alpha_2}{3}\nu\|\nabla e_{j,u}^{n}\|_f^2+\frac{C\Delta t^2}{\alpha_2\gamma^2}\|p_{j,tt}(\xi_n)\|_f^2,
\end{aligned}
\tag{45}
$$

where $\xi_n\in(t_{n-1},t_{n+1})$.

$$
\begin{aligned}
&\frac{1}{\gamma}\sum_i\int_I\left(\eta_{i,j}-\bar{\eta}_i\right)(e_{j,u}^{n}\cdot\hat{\tau}_i)(\int_{t_n}^{t_{n+1}}\mu_j(t)\,dt\cdot\hat{\tau}_i)\,ds\le\frac{1}{\gamma}\sum_i\eta_{i,j}^{\prime max}\int_I|(e_{j,u}^{n}\cdot\hat{\tau}_i)(\int_{t_n}^{t_{n+1}}\mu_j(t)\,dt\cdot\hat{\tau}_i)|\,ds \\
&\le\sum_i\left[\sigma_2\eta_i^{\prime max}\int_I(e_{j,u}^{n}\cdot\hat{\tau}_i)^2\,ds+\frac{C\eta_i^{\prime max}}{\sigma_2\gamma^2}\int_I(\int_{t_n}^{t_{n+1}}\mu_j(t)\,dt\cdot\hat{\tau}_i)^2\,ds\right] \\
&\le\sum_i\left[\sigma_2\eta_i^{\prime max}\int_I(e_{j,u}^{n}\cdot\hat{\tau}_i)^2\,ds+\frac{C\eta_i^{\prime max}}{\sigma_2\gamma^2}\Delta t\int_{t_n}^{t_{n+1}}\|\nabla\mu_j(t)\|_f^2\,dt\right] \\
&\le\sum_i\left[\sigma_2\eta_i^{\prime max}\int_I(e_{j,u}^{n}\cdot\hat{\tau}_i)^2\,ds+\frac{C\eta_i^{\prime max}}{\sigma_2\gamma^2}\Delta t\int_{t_n}^{t_{n+1}}\|p_{j,t}(t)\|_f^2\,dt\right].
\end{aligned}
\tag{46}
$$

$$
\begin{aligned}
&\frac{1}{\gamma}\sum_i\int_I\left(\eta_{i,j}-\bar{\eta}_i\right)((u_j(t_{n+1})-u_j(t_n))\cdot\hat{\tau}_i)(\int_{t_n}^{t_{n+1}}\mu_j(t)\,dt\cdot\hat{\tau}_i)\,ds \\
&\le\frac{1}{\gamma}\sum_i\eta_{i,j}^{\prime max}\int_I|((u_j(t_{n+1})-u_j(t_n))\cdot\hat{\tau}_i)(\int_{t_n}^{t_{n+1}}\mu_j(t)\,dt\cdot\hat{\tau}_i)|\,ds \\
&\le\sum_i\left[\frac{C}{\gamma}\eta_i^{\prime max}\Delta t\int_{t_n}^{t_{n+1}}\|\nabla u_{j,t}\|_f^2\,dt+\frac{C}{\gamma}\eta_i^{\prime max}\Delta t\int_{t_n}^{t_{n+1}}\|p_{j,t}(t)\|_f^2\,dt\right].
\end{aligned}
\tag{47}
$$

$$
\frac{1}{\gamma}\sum_i\int_I\bar{\eta}_i(e_{j,u}^{n+1}\cdot\hat{\tau}_i)(\int_{t_n}^{t_{n+1}}\mu_j(t)\,dt\cdot\hat{\tau}_i)\,ds \tag{48}
$$

$$\leq \sum_i \left[\sigma_3 \int_I \bar{\eta}_i (e_{j,u}^{n+1} \cdot \hat{\tau}_i)^2 ds + \frac{C\bar{\eta}_i}{\sigma_3 \gamma^2} \Delta t \int_{t_n}^{t_{n+1}} \|p_{j,t}(t)\|_f^2 \, dt \right].$$

$$\frac{1}{\gamma} c_I \left(\int_{t_n}^{t_{n+1}} \mu_j(t) \, dt, e_{j,\phi}^n \right) \leq \frac{C\Delta t}{\beta_2 \gamma^2 g \bar{k}_{min}} \int_{t_n}^{t_{n+1}} \|p_{j,t}(t)\|_f^2 + \frac{\beta_2}{2} g \bar{k}_{min} \|\nabla e_{j,\phi}^n\|^2. \tag{49}$$

Combining all these estimates, we have the following inequality

$$\begin{aligned}
&\frac{1}{2\Delta t}\|e_{j,u}^{n+1}\|_f^2 - \frac{1}{2\Delta t}\|e_{j,u}^{n}\|_f^2 + \left(1 - \alpha_1 - \alpha_2 - \Delta t \frac{2C_2}{\beta_1^2 \nu}\right) \nu \|\nabla e_{j,u}^{n+1}\|_f^2 \\
&+ \left(\frac{\alpha_2}{3}\nu + \Delta t \frac{C_2}{\beta_1^2}\right) \left(\|\nabla e_{j,u}^{n+1}\|_f^2 - \|\nabla e_{j,u}^{n}\|_f^2 \right) + \sum_i \left((1-\sigma_3)\bar{\eta}_i^{min} - (1+\sigma_1+\sigma_2)\eta_i'^{max} \right) \int_I (e_{j,u}^{n+1} \cdot \hat{\tau}_i)^2 \, ds \\
&+ \sum_i (\sigma_2 + \frac{1}{2}) \eta_i'^{max} \left(\int_I (e_{j,u}^{n+1} \cdot \hat{\tau}_i)^2 \, ds - \int_I (e_{j,u}^{n} \cdot \hat{\tau}_i)^2 \, ds \right) + \frac{gS_0}{2\Delta t}\|e_{j,\phi}^{n+1}\|_p^2 - \frac{gS_0}{2\Delta t}\|e_{j,\phi}^{n}\|_p^2 \\
&+ \left((1 - \beta_1 - \beta_2 - \Delta t \frac{2C_1}{g^2 S_0 \bar{k}_{min} \alpha_1^2}) - (1+\beta_3)\frac{\rho'_{max}}{\bar{k}_{min}} \right) g \bar{k}_{min} \|\nabla e_{j,\phi}^{n+1}\|_p^2 \\
&+ \left(\frac{\beta_2}{2} g \bar{k}_{min} + \frac{1}{2} g \rho'_{max} + \frac{\Delta t C_1}{g S_0 \alpha_1^2} \right) \left(\|\nabla e_{j,\phi}^{n+1}\|_p^2 - \|\nabla e_{j,\phi}^{n}\|_p^2 \right) + \frac{1}{2\gamma} \left(\|e_{j,p}^{n+1}\|_f^2 - \|e_{j,p}^{n}\|_f^2 \right) + \frac{1}{2\gamma} \|e_{j,p}^{n+1} - e_{j,p}^{n}\|_f^2 \\
&\leq \sum_i \frac{C}{\sigma_1} \eta_i'^{max} \Delta t \int_{t^n}^{t^{n+1}} \|\nabla u_{j,t}\|_f^2 \, dt + C\Delta t \int_{t^n}^{t^{n+1}} \|u_{j,tt}\|_f^2 \, dt + C\Delta t \int_{t^n}^{t^{n+1}} \|\nabla \phi_{j,t}\|_p^2 \, dt \\
&+ C\Delta t \int_{t^n}^{t^{n+1}} \|\phi_{j,tt}\|_p^2 \, dt + C\Delta t \int_{t^n}^{t^{n+1}} \|\nabla u_{j,t}\|_f^2 \, dt + \frac{Cg\rho'_{max}}{\beta_3} \Delta t \int_{t^n}^{t^{n+1}} \|\nabla \phi_{j,t}\|_p^2 \, dt \\
&+ C\Delta t \int_{t^n}^{t^{n+1}} \|u_{j,tt}(t)\|_f^2 \, dt + C\Delta t \int_{t^n}^{t^{n+1}} \|\nabla \phi_{j,t}(t)\|_p^2 \, dt + \frac{C}{\gamma} \nu \Delta t \int_{t_n}^{t_{n+1}} \|p_{j,t}(t)\|_f^2 dt \\
&+ \frac{C\nu\Delta t}{\alpha_2 \gamma^2} \int_{t_n}^{t_{n+1}} \|p_{j,t}(t)\|_f^2 dt + \frac{1}{\gamma \Delta t} \left[\left(e_{j,u}^{n+1}, \int_{t_n}^{t_{n+1}} \mu_j(t) \, dt \right)_f - \left(e_{j,u}^{n}, \int_{t_{n-1}}^{t_n} \mu_j(t) \, dt \right)_f \right] \\
&+ \frac{C\Delta t^2}{\alpha_2 \gamma^2} \|p_{j,tt}(\xi_n)\|_f^2 + \sum_i \left(\frac{C\eta_i'^{max}}{\sigma_2 \gamma^2} + \frac{C\bar{\eta}_i}{\sigma_3 \gamma^2} \right) \Delta t \int_{t_n}^{t_{n+1}} \|p_{j,t}(t)\|_f^2 \, dt \\
&+ \sum_i \left[\frac{C}{\gamma} \eta_i'^{max} \Delta t \int_{t_n}^{t_{n+1}} \|\nabla u_{j,t}\|_f^2 \, dt + \frac{C}{\gamma} \eta_i'^{max} \Delta t \int_{t_n}^{t_{n+1}} \|p_{j,t}(t)\|_f^2 \, dt \right] + \frac{C\Delta t}{\beta_2 \gamma^2 g \bar{k}_{min}} \int_{t_n}^{t_{n+1}} \|p_{j,t}(t)\|_f^2.
\end{aligned} \tag{50}$$

To make sure the third, fifth and ninth term on the left hand side are non-negative, we need $0 < \alpha_1, \alpha_2, \sigma_3, \beta_1, \beta_2 < 1$, and

$$\frac{\eta_i'^{max}}{\bar{\eta}_i^{min}} \leq \frac{1 - \sigma_3}{1 + \sigma_1 + \sigma_2}, \qquad \frac{\rho'_{max}}{\bar{k}_{min}} < \frac{1}{1 + \beta_3}. \tag{51}$$

For $\forall \sigma_3 \in (0,1), \forall \sigma_1 > 0, \forall \sigma_2 > 0, \forall \beta_3 > 0$, we can derive that $\frac{1-\sigma_3}{1+\sigma_1+\sigma_2}, \frac{1}{1+\beta_3} \in (0,1)$. Now if the two parameter conditions in (8) are satisfied, we have $\frac{\eta_i'^{max}}{\bar{\eta}_i^{min}}, \frac{\rho'_{max}}{\bar{k}_{min}} \in (0,1)$. Then we can easily find $\sigma_3 \in (0,1), \sigma_1 > 0, \sigma_2 > 0$ such that $\frac{\eta_i'^{max}}{\bar{\eta}_i^{min}} = \frac{1-\sigma_3}{1+\sigma_1+\sigma_2}$, and $\beta_3 > 0$ such that $\frac{\rho'_{max}}{\bar{k}_{min}} < \frac{1}{1+\beta_3}$.

Then under the two parameter conditions in (26), and the time-step condition (25), (50) reduces to

$$\begin{aligned}
&\frac{1}{2\Delta t}\|e_{j,u}^{n+1}\|_f^2-\frac{1}{2\Delta t}\|e_{j,u}^{n}\|_f^2+(\frac{\alpha_2}{3}\nu+\Delta t\frac{C_2}{\beta_1^2})\left(\|\nabla e_{j,u}^{n+1}\|_f^2-\|\nabla e_{j,u}^{n}\|_f^2\right) \\
&+\sum_i(\sigma_2+\frac{1}{2})\eta_i'^{max}\left(\int_I(e_{j,u}^{n+1}\cdot\hat{\tau}_i)^2\,ds-\int_I(e_{j,u}^{n}\cdot\hat{\tau}_i)^2\,ds\right)+\frac{gS_0}{2\Delta t}\|e_{j,\phi}^{n+1}\|_p^2-\frac{gS_0}{2\Delta t}\|e_{j,\phi}^{n}\|_p^2 \\
&+\left(\frac{\beta_2}{2}g\bar{k}_{min}+\frac{1}{2}g\rho'_{max}+\frac{\Delta tC_1}{gS_0\alpha_1^2}\right)\left(\|\nabla e_{j,\phi}^{n+1}\|_p^2-\|\nabla e_{j,\phi}^{n}\|_p^2\right)+\frac{1}{2\gamma}\left(\|e_{j,p}^{n+1}\|_f^2-\|e_{j,p}^{n}\|_f^2\right)+\frac{1}{2\gamma}\|e_{j,p}^{n+1}-e_{j,p}^{n}\|_f^2 \\
&\le\sum_i\frac{C}{\sigma_1}\eta_i'^{max}\Delta t\int_{t^n}^{t^{n+1}}\|\nabla u_{j,t}\|_f^2\,dt+C\Delta t\int_{t^n}^{t^{n+1}}\|u_{j,tt}\|_f^2\,dt+C\Delta t\int_{t^n}^{t^{n+1}}\|\nabla\phi_{j,t}\|_p^2\,dt \\
&+C\Delta t\int_{t^n}^{t^{n+1}}\|\phi_{j,tt}\|_p^2\,dt+C\Delta t\int_{t^n}^{t^{n+1}}\|\nabla u_{j,t}\|_f^2\,dt+\frac{Cg\rho'_{max}}{\beta_3}\Delta t\int_{t^n}^{t^{n+1}}\|\nabla\phi_{j,t}\|_p^2\,dt \\
&+C\Delta t\int_{t^n}^{t^{n+1}}\|u_{j,tt}(t)\|_f^2\,dt+C\Delta t\int_{t^n}^{t^{n+1}}\|\nabla\phi_{j,t}(t)\|_p^2\,dt+\frac{C}{\gamma}\nu\Delta t\int_{t_n}^{t_{n+1}}\|p_{j,t}(t)\|_f^2dt \\
&+\frac{C\nu\Delta t}{\alpha_2\gamma^2}\int_{t_n}^{t_{n+1}}\|p_{j,t}(t)\|_f^2dt+\frac{1}{\gamma\Delta t}\left[\left(e_{j,u}^{n+1},\int_{t_n}^{t_{n+1}}\mu_j(t)\,dt\right)_f-\left(e_{j,u}^{n},\int_{t_{n-1}}^{t_n}\mu_j(t)\,dt\right)_f\right] \\
&+\frac{C\Delta t^2}{\alpha_2\gamma^2}\|p_{j,tt}(\xi_n)\|_f^2+\sum_i\left(\frac{C\eta_i'^{max}}{\sigma_2\gamma^2}+\frac{C\bar{\eta}_i}{\sigma_3\gamma^2}\right)\Delta t\int_{t_n}^{t_{n+1}}\|p_{j,t}(t)\|_f^2\,dt \\
&+\sum_i\left[\frac{C}{\gamma}\eta_i'^{max}\Delta t\int_{t_n}^{t_{n+1}}\|\nabla u_{j,t}\|_f^2\,dt+\frac{C}{\gamma}\eta_i'^{max}\Delta t\int_{t_n}^{t_{n+1}}\|p_{j,t}(t)\|_f^2\,dt\right]+\frac{C\Delta t}{\beta_2\gamma^2g\bar{k}_{min}}\int_{t_n}^{t_{n+1}}\|p_{j,t}(t)\|_f^2.
\end{aligned}\tag{52}$$

Since $e_{j,u}^0=0$, $e_{j,p}^0=0$, and $e_{j,\phi}^0=0$, summing up (52) from $n=0$ to $n=N-1$ and multiplying through by Δt yields

$$\begin{aligned}
&\frac{1}{2}\|e_{j,u}^{N}\|_f^2+(\frac{\alpha_2}{3}\nu\Delta t+\Delta t^2\frac{C_2}{\beta_1^2})\|\nabla e_{j,u}^{N}\|_f^2+\sum_i(\sigma_2+\frac{1}{2})\Delta t\eta_i'^{max}\int_I(e_{j,u}^{N}\cdot\hat{\tau}_i)^2\,ds+\frac{gS_0}{2}\|e_{j,\phi}^{N}\|_p^2 \\
&+\left(\frac{\beta_2}{2}g\bar{k}_{min}+\frac{1}{2}g\rho'_{max}+\frac{\Delta tC_1}{gS_0\alpha_1^2}\right)\Delta t\|\nabla e_{j,\phi}^{N}\|_p^2+\frac{1}{2\gamma}\Delta t\|e_{j,p}^{N}\|_f^2+\sum_{n=0}^{N-1}\frac{1}{2\gamma}\Delta t\|e_{j,p}^{n+1}-e_{j,p}^{n}\|_f^2 \\
&\le\Delta t\sum_{n=0}^{N-1}\Bigg\{\sum_i\frac{C}{\sigma_1}\eta_i'^{max}\Delta t\int_{t^n}^{t^{n+1}}\|\nabla u_{j,t}\|_f^2\,dt+C\Delta t\int_{t^n}^{t^{n+1}}\|u_{j,tt}\|_f^2\,dt+C\Delta t\int_{t^n}^{t^{n+1}}\|\nabla\phi_{j,t}\|_p^2\,dt \\
&+C\Delta t\int_{t^n}^{t^{n+1}}\|\phi_{j,tt}\|_p^2\,dt+C\Delta t\int_{t^n}^{t^{n+1}}\|\nabla u_{j,t}\|_f^2\,dt+\frac{Cg\rho'_{max}}{\beta_3}\Delta t\int_{t^n}^{t^{n+1}}\|\nabla\phi_{j,t}\|_p^2\,dt \\
&+C\Delta t\int_{t^n}^{t^{n+1}}\|u_{j,tt}(t)\|_f^2\,dt+C\Delta t\int_{t^n}^{t^{n+1}}\|\nabla\phi_{j,t}(t)\|_p^2\,dt+\frac{C}{\gamma}\nu\Delta t\int_{t_n}^{t_{n+1}}\|p_{j,t}(t)\|_f^2dt \\
&+\frac{C\nu\Delta t}{\alpha_2\gamma^2}\int_{t_n}^{t_{n+1}}\|p_{j,t}(t)\|_f^2dt+\frac{C\Delta t^2}{\alpha_2\gamma^2}\|p_{j,tt}(\xi_n)\|_f^2+\sum_i\left(\frac{C\eta_i'^{max}}{\sigma_2\gamma^2}+\frac{C\bar{\eta}_i}{\sigma_3\gamma^2}\right)\Delta t\int_{t_n}^{t_{n+1}}\|p_{j,t}(t)\|_f^2\,dt
\end{aligned}\tag{53}$$

$$+\sum_i\left[\frac{C}{\gamma}\eta_i'^{max}\Delta t\int_{t_n}^{t_{n+1}}\|\nabla u_{j,t}\|_f^2\,dt+\frac{C}{\gamma}\eta_i'^{max}\Delta t\int_{t_n}^{t_{n+1}}\|p_{j,t}(t)\|_f^2\,dt\right]+\frac{C\Delta t}{\beta_2\gamma^2 g\bar{k}_{min}}\int_{t_n}^{t_{n+1}}\|p_{j,t}(t)\|_f^2\Big\}$$
$$+\frac{1}{\gamma}\left(e_{j,u}^N,\int_{t_{N-1}}^{t_N}\mu_j(t)\,dt\right)_f.$$

The last term in (53) can be bounded as

$$\frac{1}{\gamma}\left(e_{j,u}^N,\int_{t_{N-1}}^{t_N}\mu_j(t)\,dt\right)_f=\frac{\Delta t}{\gamma}\left(e_{j,u}^N,\mu_j(\theta_N)\right)_f\le\frac{1}{4}\|e_{j,u}^N\|_f^2+\frac{\Delta t^2}{\gamma^2}\|\mu_j(\theta_N)\|_f^2 \tag{54}$$
$$\le\frac{1}{4}\|e_{j,u}^N\|_f^2+C\Delta t^2\|p_{j,t}(\theta_N)\|_f^2\le\frac{1}{4}\|e_{j,u}^N\|_f^2+C\Delta t^2\|p_{j,t}\|_{\infty,0,f}^2,$$

where $\theta_N\in(t_{N-1},t_N)$.

Moreover, for functions $v(x,t)$ defined on $D_f\times(-T,T)$, we define the norm

$$\|v\|_{\infty^*,0,f}:=\|v\|_{L^\infty(-T,T;L^2(D_f))}.$$

Then the second term at sixth line of (53) can be bounded as follows.

$$\Delta t\sum_{n=1}^{N-1}\frac{C\Delta t^2}{\alpha_2\gamma^2}\|p_{j,tt}(\xi_n)\|_f^2\le C\Delta t^2\|p_{j,tt}\|_{\infty^*,0,f}^2. \tag{55}$$

Then (53) reduces to

$$\frac{1}{2}\|e_{j,u}^N\|_f^2+(\frac{\alpha_2}{3}\nu\Delta t+\Delta t^2\frac{C_2}{\beta_1^2})\|\nabla e_{j,u}^N\|_f^2+\sum_i(\sigma_2+\frac{1}{2})\Delta t\eta_i'^{max}\int_I(e_{j,u}^N\cdot\hat{\tau}_i)^2\,ds+\frac{gS_0}{2}\|e_{j,\phi}^N\|_p^2 \tag{56}$$
$$+\left(\frac{\beta_2}{2}g\bar{k}_{min}+\frac{1}{2}g\rho'_{max}+\frac{\Delta tC_1}{gS_0\alpha_1^2}\right)\Delta t\|\nabla e_{j,\phi}^N\|_p^2+\frac{1}{2\gamma}\Delta t\|e_{j,p}^N\|_f^2+\sum_{n=0}^{N-1}\frac{1}{2\gamma}\Delta t\|e_{j,p}^{n+1}-e_{j,p}^n\|_f^2$$
$$\le C\Delta t^2\|u_{j,t}\|_{2,1,f}^2+C\Delta t^2\|u_{j,tt}\|_{2,0,f}^2+C\Delta t^2\|\phi_{j,t}\|_{2,1,p}^2+C\Delta t^2\|\phi_{j,tt}\|_{2,0,p}^2+C\Delta t^2\|p_{j,t}(t)\|_{2,0,f}^2$$
$$+C\Delta t^2\|p_{j,tt}\|_{\infty^*,0,f}^2+C\Delta t^2\|p_{j,t}\|_{\infty,0,f}^2\le C\Delta t^2.$$

□

5 | NUMERICAL ILLUSTRATIONS

In this section, the features of the proposed AC ensemble scheme for the Stokes-Darcy system are shown by three examples of numerical experiments. The first example is to test the convergence of the ensemble algorithm with a known exact solution. In order to show how to combine our ensemble algorithm with the Monte Carlo method to solve the Stokes-Darcy system with a random hydraulic conductivity tensor efficiently, we present the second example, which also shows the efficiency and effectiveness of the AC ensemble algorithm by comparing the numerical results and computation time with those of the individual simulations. In the third example we apply the proposed algorithm to a realistic simulation of the subsurface flow in a karst aquifer.

To discretize the Stokes-Darcy problem in space by the finite element method, we choose conforming velocity, pressure, hydraulic head finite element spaces based on an edge to edge triangulation ($d=2$) of the domain $D_{f/p}$ with maximum element diameter h. The continuity across the interface I between the finite element meshes in the two subdomains is not assumed. Taylor-Hood elements,[72], which satisfy the usual discrete inf-sup $/LBB^h$ condition for stability of the discrete pressure, are used in following numerical tests for approximation of the Stokes equations. The continuous piecewise quadratic finite elements are used for the approximation of the Darcy equation.

5.1 | Stability and convergence test

In order to illustrate the convergence rate of our AC ensemble algorithm, we compute the numerical error between the numerical approximation and a known exact solution. First, we consider the model problem on $D = [0, \pi] \times [-1, 1]$, where $D_p = [0, \pi] \times [-1, 0]$, and $D_f = [0, \pi] \times [0, 1]$. We take $\alpha_{BJS} = 1$, $\nu = 1$, $g = 1$, $S_0 = 1$. The boundary condition functions and the source terms are chosen such that the following functions are the exact solutions:

$$\begin{aligned} \phi &= (e^y - e^{-y}) sin(x) e^t, \\ u &= [\frac{k_{11}^j}{\pi} sin(2\pi y) cos(x), (-2k_{22}^j + \frac{k_{22}^j}{\pi^2} sin^2(\pi y)) sin(x)]^T e^t, \\ p &= sin(\pi x y) e^t. \end{aligned}$$

For the hydraulic conductivity tensor, we set

$$\mathcal{K} = \mathcal{K}_j = \begin{bmatrix} k_{11}^j & 0 \\ 0 & k_{22}^j \end{bmatrix}, \quad j = 1, \dots, J,$$

where $\mathcal{K}_j$ is one of the samples of $\mathcal{K}$. In this simple test, we only consider the case that k_{11}, k_{22} are random variables independent of spatial coordinates. All the numerical results below are for $t = T = 1$.

We consider a group of simulations with $J = 3$ members. The three members are corresponding to different hydraulic conductivity tensors, i.e. $k_{11}^1 = k_{22}^1 = 1e^{-3}, k_{11}^2 = k_{22}^2 = 0.9e^{-3}, k_{11}^3 = k_{22}^3 = 1.1e^{-3}$. As $\mathcal{K}$ is diagonal, we use Algorithm 2 for computation, and thus there are no parameter conditions for both stability and convergence. In order to check the convergence order in time, we uniformly refine the mesh size h and time step size Δt from the initial mesh size $1/4$ and time step size $\Delta t = 0.1h$. The approximation errors of the AC ensemble method are listed in Table 1, Table 2 and Table 3, for the velocity $\vec{u}$, the hydraulic head ϕ and the pressure p respectively. From these tables, we can find that our ensemble algorithm is first order convergence in time. Next we set time step size $\Delta t = 8h^3$ and we can obtain the approximation errors of the ensemble method in Table 4, Table 5 and Table 6, for the velocity u, the hydraulic head ϕ and the pressure p respectively. From these tables, we can find the rate of convergence is $O(h^3 + \triangle t) = O(h^3) = O(\Delta t)$ with respect to L^2 norms for u and ϕ.

TABLE 1 Errors and convergence rates of the AC ensemble algorithm ($J = 3$) for $\triangle t = 0.1h$.

h	$\|u_h - u\|_0^{E,1}$	rate	$\|u_h - u\|_0^{E,2}$	rate	$\|u_h - u\|_0^{E,3}$	rate
1/4	6.199×10^{-2}	–	6.189×10^{-2}	–	6.200×10^{-2}	–
1/8	2.944×10^{-2}	1.07	2.906×10^{-2}	1.09	2.924×10^{-2}	1.08
1/16	1.408×10^{-2}	1.06	1.377×10^{-2}	1.07	1.469×10^{-2}	0.99
1/32	6.935×10^{-3}	1.02	6.784×10^{-3}	1.02	7.348×10^{-3}	1.00
1/64	3.287×10^{-3}	1.11	3.230×10^{-3}	1.10	3.661×10^{-3}	1.00
h	$\|u_h - u\|_1^{E,1}$	rate	$\|u_h - u\|_1^{E,2}$	rate	$\|u_h - u\|_1^{E,3}$	rate
1/4	1.259×10^{-1}	–	1.248×10^{-1}	–	1.260×10^{-1}	–
1/8	5.246×10^{-2}	1.26	5.403×10^{-2}	1.20	5.612×10^{-2}	1.21
1/16	2.385×10^{-2}	1.13	2.573×10^{-2}	1.07	2.647×10^{-2}	0.96
1/32	1.135×10^{-2}	1.07	1.169×10^{-2}	1.13	1.260×10^{-2}	1.07
1/64	5.405×10^{-3}	1.10	5.874×10^{-3}	0.99	6.331×10^{-3}	0.99

5.2 | Convergence and efficiency test for J random samples

We next consider using the presented ensemble algorithm for approximating stochastic Stokes-Darcy equations with a random hydraulic conductivity tensor $\mathcal{K}(x, w)$ that depends on spatial coordinates. Let $(\Omega, \mathcal{F}, \mathcal{P})$ be a complete probability space. Here Ω is the set of outcomes, $\mathcal{F} \in 2^\Omega$ is the $\sigma-$algebra of events, and $\mathcal{P} : \mathcal{F} \to [0, 1]$ is a probability measure. The stochastic

TABLE 2 Errors and convergence rates of the AC ensemble algorithm ($J = 3$) for $\triangle t = 0.1h$.

h	$\|\phi_h - \phi\|_0^{E,1}$	rate	$\|\phi_h - \phi\|_0^{E,2}$	rate	$\|\phi_h - \phi\|_0^{E,3}$	rate
1/4	1.799×10^{-1}	–	1.780×10^{-1}	–	1.800×10^{-1}	–
1/8	8.177×10^{-2}	1.13	8.091×10^{-2}	1.13	8.372×10^{-2}	1.10
1/16	3.894×10^{-2}	1.07	3.799×10^{-2}	1.09	3.987×10^{-2}	1.07
1/32	1.928×10^{-2}	1.01	1.809×10^{-2}	1.07	1.954×10^{-2}	1.03
1/64	9.181×10^{-3}	1.10	9.090×10^{-3}	1.00	9.304×10^{-3}	1.10
h	$\|\phi_h - \phi\|_1^{E,1}$	rate	$\|\phi_h - \phi\|_1^{E,2}$	rate	$\|\phi_h - \phi\|_1^{E,3}$	rate
1/4	4.620×10^{-1}	–	4.599×10^{-1}	–	4.625×10^{-1}	–
1/8	2.090×10^{-1}	1.14	2.169×10^{-1}	1.08	2.171×10^{-1}	1.09
1/16	9.955×10^{-2}	1.07	1.033×10^{-1}	1.07	4.337×10^{-2}	1.07
1/32	4.953×10^{-2}	1.11	5.139×10^{-2}	1.00	1.086×10^{-3}	1.09
1/64	2.359×10^{-2}	1.10	2.582×10^{-2}	0.99	5.485×10^{-4}	0.98

TABLE 3 Errors and convergence rates of the AC ensemble algorithm ($J = 3$) for $\triangle t = 0.1h$.

h	$\|p_h - p\|_0^{E,1}$	rate	$\|p_h - p\|_0^{E,2}$	rate	$\|p_h - p\|_0^{E,3}$	rate
1/4	5.558×10^{-1}	–	5.578×10^{-1}	–	5.577×10^{-1}	–
1/8	2.316×10^{-1}	1.25	2.425×10^{-1}	1.20	2.403×10^{-1}	1.21
1/16	1.007×10^{-1}	1.20	1.097×10^{-1}	1.14	1.145×10^{-1}	1.06
1/32	4.536×10^{-2}	1.15	4.989×10^{-2}	1.13	5.451×10^{-2}	1.07
1/64	2.160×10^{-2}	1.10	2.507×10^{-2}	0.99	2.739×10^{-2}	0.99

Stokes-Darcy system considered reads: Find the functions $u : D_f \times [0,T] \times \Omega \to \mathbb{R}^d$ $(d = 2, 3)$, $p : D_f \times [0,T] \times \Omega \to \mathbb{R}$, and $\phi : D_p \times [0,T] \times \Omega \to \mathbb{R}$, such that it holds $\mathcal{P} - a.e.$ in Ω, or in other words, almost surely

$$\begin{aligned} u_t(x,t,\omega) - \nu\Delta u(x,t,\omega) + \nabla p(x,t,\omega) &= f_f(x,t), \quad \nabla \cdot u(x,t,\omega) = 0, \ \text{ in } D_f \times \Omega \\ S_0\phi_t(x,t,\omega) - \nabla \cdot (\mathcal{K}(x,\omega)\nabla\phi(x,t,\omega)) &= f_p(x,t), \ \text{ in } D_p \times \Omega, \\ \phi(x,0) = \phi_0(x), \ \text{ in } D_p, \ \text{ and } u(x,0) &= u_0(x), \ \text{ in } D_f, \\ \phi(x,t,\omega) = 0, \ \text{ in } \partial D_p \backslash I \text{ and } u(x,t,\omega) &= 0, \ \text{ in } \partial D_f \backslash I, \end{aligned} \tag{57}$$

where $f_f(x,t) \in L^2(D_f)$, $f_p(x,t) \in L^2(D_p)$. The hydraulic conductivity $\mathcal{K}(x,\omega)$ is a stochastic function, which is assumed to have continuous and bounded correlation function.

We construct the random hydraulic conductivity tensor that varies in the vertical direction as follows

$$\mathcal{K}(\vec{x},\omega) = \begin{bmatrix} k_{11}(\vec{x},\omega) & 0 \\ 0 & k_{22}(\vec{x},\omega) \end{bmatrix}, \quad \text{and}$$

$$k_{11}(\vec{x},\omega) = k_{22}(\vec{x},\omega) = k(\vec{x},\omega) = a_0 + \sigma\sqrt{\lambda_0}Y_0(\omega) + \sum_{i=1}^{n_f} \sigma\sqrt{\lambda_i}[Y_i(\omega)cos(i\pi y) + Y_{n_f+i}(\omega)sin(i\pi y)],$$

where $\vec{x} = (x,y)^T$, $\lambda_0 = \frac{\sqrt{\pi}L_c}{2}$, $\lambda_i = \sqrt{\pi}L_c e^{-\frac{(i\pi L_c)^2}{4}}$ for $i = 1, \ldots, n_f$ and $Y_0, \ldots, Y_{2n_f}$ are uncorrelated random variables with zero mean and unit variance. In the following numerical test, we take the desired physical correlation length $L_c = 0.25$ for the random field and $a_0 = 1$, $\sigma = 0.15$, $n_f = 3$. We assume the random variables $Y_0, \ldots, Y_{2n_f}$ are independent and uniformly distributed in the interval $[-\sqrt{3}, \sqrt{3}]$. Note that in this setting, the random functions $k_{11}(\vec{x},w), k_{22}(\vec{x},w)$ are guaranteed to be positive, and the corresponding $\mathcal{K}(\vec{x},\omega)$ is SPD.

TABLE 4 Errors and convergence rates of the ensemble algorithm ($J = 3$) for $\triangle t = 8h^3$.

h	$\|u_h - u\|_0^{E,1}$	rate	$\|u_h - u\|_0^{E,2}$	rate	$\|u_h - u\|_0^{E,3}$	rate
1/4	1.0498×10^{-2}	–	1.0491×10^{-2}	–	1.0504×10^{-2}	–
1/8	1.0382×10^{-3}	3.33	1.0376×10^{-3}	3.34	1.0389×10^{-3}	3.33
1/16	1.2457×10^{-4}	3.06	1.2422×10^{-4}	3.06	1.2471×10^{-4}	3.05
1/32	1.6161×10^{-5}	2.95	1.5316×10^{-5}	3.01	1.5089×10^{-5}	3.04
1/64	2.0226×10^{-6}	3.00	1.9098×10^{-6}	3.00	1.9328×10^{-6}	3.00

h	$\|u_h - u\|_1^{E,1}$	rate	$\|u_h - u\|_1^{E,2}$	rate	$\|u_h - u\|_1^{E,3}$	rate
1/4	1.4414×10^{-1}	–	1.4413×10^{-1}	–	1.4521×10^{-1}	–
1/8	2.5258×10^{-2}	2.51	2.5253×10^{-2}	2.51	2.5338×10^{-2}	2.51
1/16	6.1305×10^{-3}	2.04	6.1443×10^{-3}	2.04	6.1801×10^{-3}	2.03
1/32	1.4527×10^{-3}	2.07	1.4527×10^{-3}	2.07	1.4679×10^{-3}	2.07
1/64	3.5173×10^{-4}	2.04	3.5256×10^{-4}	2.03	3.5717×10^{-4}	2.04

TABLE 5 Errors and convergence rates of the ensemble algorithm ($J = 3$) for $\triangle t = 8h^3$.

h	$\|\phi_h - \phi\|_0^{E,1}$	rate	$\|\phi_h - \phi\|_0^{E,2}$	rate	$\|\phi_h - \phi\|_0^{E,3}$	rate
1/4	1.6273×10^{-1}	–	1.6307×10^{-1}	–	1.6243×10^{-1}	–
1/8	2.0399×10^{-2}	3.00	2.0453×10^{-2}	3.00	2.0351×10^{-2}	3.00
1/16	2.5524×10^{-3}	3.00	2.5148×10^{-3}	3.02	2.5438×10^{-3}	3.00
1/32	3.1511×10^{-4}	3.02	3.1396×10^{-4}	3.00	3.1798×10^{-4}	3.00
1/64	3.9290×10^{-5}	3.00	3.8760×10^{-5}	3.01	3.9792×10^{-5}	2.99

h	$\|\phi_h - \phi\|_1^{E,1}$	rate	$\|\phi_h - \phi\|_1^{E,2}$	rate	$\|\phi_h - \phi\|_1^{E,3}$	rate
1/4	1.1149×10^{0}	–	1.1243×10^{0}	–	1.1063×10^{0}	–
1/8	1.8023×10^{-1}	2.63	1.8309×10^{-1}	2.61	1.7783×10^{-1}	2.63
1/16	2.8403×10^{-2}	2.66	2.8964×10^{-2}	2.66	2.8370×10^{-2}	2.64
1/32	6.9276×10^{-3}	2.03	6.9510×10^{-2}	2.06	6.7858×10^{-3}	2.06
1/64	1.7276×10^{-3}	2.00	1.7847×10^{-3}	1.97	1.7213×10^{-4}	1.98

The domain and parameters are the same as those in the first test. But in this test, the problem is associated with the forcing terms as follows:

$$f_p = (e^y - e^{-y})sin(x)e^t,$$
$$f_{f_1} = [(1 + \nu + 4\nu\pi^2)\frac{k(\vec{x},\omega)}{\pi}]sin(2\pi y)cos(x)e^t + \pi ycos(\pi xy)e^t,$$
$$f_{f_2} = -2\nu k(\vec{x},\omega)cos(2\pi y)sin(x)e^t + (1+\nu)[-2k(\vec{x},\omega) + \frac{k(\vec{x},\omega)}{\pi^2}sin^2(\pi y)]sin(x)e^t + \pi xcos(\pi xy)e^t.$$

The Dirichlet boundary condition

$$\phi = (e^y - e^{-y})sin(x)e^t,$$
$$u = [\frac{k(\vec{x},\omega)}{\pi}sin(2\pi y)cos(x), (-2k(\vec{x},\omega) + \frac{k(\vec{x},\omega)}{\pi^2}sin^2(\pi y))sin(x)]^T e^t,$$

will be used on the boundary of the domain, and the initial conditions are chosen by

$$\phi = (e^y - e^{-y})sin(x),$$

TABLE 6 Errors and convergence rates of the ensemble algorithm ($J = 3$) for $\triangle t = 8h^3$.

h	$\|p_h - p\|_0^{E,1}$	rate	$\|p_h - p\|_0^{E,2}$	rate	$\|p_h - p\|_0^{E,3}$	rate
1/4	4.8777×10^{-1}	–	4.8779×10^{-1}	–	4.8694×10^{-1}	–
1/8	1.1482×10^{-1}	2.08	1.1481×10^{-1}	2.08	1.1478×10^{-1}	2.08
1/16	2.6003×10^{-2}	2.14	2.6003×10^{-2}	2.14	2.8695×10^{-2}	2.00
1/32	6.2658×10^{-3}	2.05	6.8315×10^{-3}	1.93	6.9987×10^{-3}	2.03
1/64	1.5245×10^{-3}	2.04	1.6589×10^{-3}	2.04	1.6987×10^{-3}	2.04

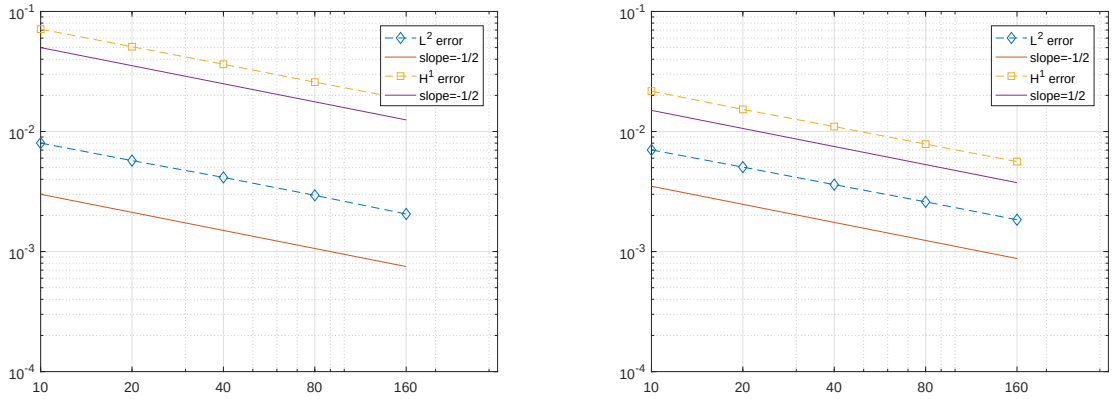

FIGURE 2 Ensemble simulations errors are $O(1/\sqrt{J})$ for u (left) and ϕ (right).

$$u = [\frac{k(\vec{x},\omega)}{\pi} sin(2\pi y)cos(x), (-2k(\vec{x},\omega) + \frac{k(\vec{x},\omega)}{\pi^2} sin^2(\pi y))sin(x)]^T,$$
$$p = sin(\pi xy).$$

We simulate the system over the time interval $[0, 0.5]$, and the uniform triangulation with mesh size $h = 1/32$ and uniform time partition with time step size $\Delta t = 0.1h$ are used. We generate a set of J random samples of $\mathcal{K}$ by the Monte Carlo sampling, and run our code for simulating the ensemble of the system associated with the J realizations. First, we need to check the rate of convergence with respect to the numbers of samples, J. Since $\mathcal{K}$ is diagonal, Algorithm 2 is used for ensemble computation.

We use the multifrontal LU factorization as the linear solver. Even though the back substitution stage of LU decomposition is different for different realizations, the decomposition stage of the two common matrices in the proposed method is the same for all the realizations, hence needs to to be done only once before the back substitution stage. This feature significantly saves the computational cost.

As the exact solution to the stochastic Stokes-Darcy system is unknown, we take the ensemble mean of numerical solutions of $J_0 = 1000$ realizations as our exact solution (expectation), which is denoted by u_{J_0}. We also define u_h as the ensemble mean of J realizations. The numerical results with $J = 10, 20, 40, 80, 160$ realizations are listed in Table 7. Using linear regression, the errors in Table 7 satisfy

$$\|u_h - u_{J_0}\|_0 \approx 0.0248J^{-0.4985}, \quad \|u_h - u_{J_0}\|_1 \approx 0.2183J^{-0.4864},$$
$$\|p_h - p_{J_0}\|_0 \approx 0.0214J^{-0.5033}, \quad \|\phi_h - \phi_{J_0}\|_0 \approx 0.0650J^{-0.4825}.$$

The values of $\|\cdot\|_0$ and $\|\cdot\|_1$ together with their linear regression models are plotted in Figure 2. It is seen that the rate of convergence with respect to J is close to -0.5.

Next, we briefly discuss the efficiency of our AC ensemble algorithm compared with the traditional method that runs the simulations individually, based on a test with $J = 1000$ ensemble members and the mesh size $h = 1/64$. A comparison between the matrix systems of these two methods is presented in Table 8. First, because all the realizations in our ensemble method share

TABLE 7 Errors of ensemble simulations.

J	10	20	40	80	160
$\|u_h - u_{J_0}\|_0^E$	8.0121×10^{-3}	5.7229×10^{-3}	4.1470×10^{-3}	2.9411×10^{-3}	2.0559×10^{-3}
$\|u_h - u_{J_0}\|_1^E$	7.1225×10^{-2}	5.0867×10^{-2}	3.6343×10^{-2}	2.5775×10^{-2}	1.8543×10^{-2}
$\|\phi_h - \phi_{J_0}\|_0^E$	7.0235×10^{-3}	5.0528×10^{-3}	3.6091×10^{-3}	2.5964×10^{-3}	1.8414×10^{-3}
$\|\phi_h - \phi_{J_0}\|_1^E$	2.1714×10^{-2}	1.5291×10^{-2}	1.1001×10^{-2}	7.8578×10^{-3}	5.6127×10^{-3}

the two common matrices, which are assembled only once, the cost for the matrix assembly is significantly reduced. This can be easily observed in the third column of Table 8. Secondly, the common matrix can provide opportunities to preprocess the matrix systems for all the realizations in a unified way, depending on the chosen matrix solver, such as the LU decomposition discussed above. This may lead to a significant reduction of the computational cost for solving the matrix systems. Thirdly, even though each realization in our method has two matrix systems to solve, each of these two matrices, which arise from the two level decoupling technique in the proposed method, is much smaller than the only one matrix in the traditional coupled method. Therefore, our method saves a lot of computational cost for solving the linear matrix systems.

TABLE 8 Solver comparison of ensemble simulations with traditional method

	matrix size	*number of matrix assembly*	*number of matrix solving*
individual	54148×54148	1000	1000
$ensemble_{AC}$	33282×33282	1	1000
	16641×16641	1	1000

Setting $\Delta t = 1/160$, we first run the ensemble simulations with $J = 1, 10, 20, 40, 80$ realizations using our ensemble algorithm and record the respective elapsed CPU time (in seconds), i.e., AC ensemble in Table 9. Then we run the simulations again with the same samples by using the traditional individual coupled method and record the respective elapsed CPU time, i.e., individual in Table 9. From the comparison of the elapsed CPU times presented in Table 9, one can clearly see that the proposed ensemble algorithm is much faster than the traditional approach. For example, when $J = 80$, the ensemble method saves about 95.16% of the computational time compared with the traditional method.

TABLE 9 CPU elapsed times of ensemble simulations.

J	1	10	20	40	80
individual	1177	11760	23541	47066	94132
$ensemble_{AC}$	934	1861	3290	3724	4560

Next we test our ensemble algorithm against the non-iterative multi-physics domain decomposition method (NIDDM)[14], which is more efficient than the coupled approach in the previous test for individual runs. For the hydraulic conductivity tensor, we generate uniformly distributed random numbers in $[1, 1.5]$ for k. Setting $h = 1/32$, we take the mean of numerical solutions of $J_0 = 1000$ as the exact solutions, which are denoted by u_{J_0} and ϕ_{J_0}. In Table 10 which is obtained by running the test samples for $J = 160$, NIDDM and the AC ensemble method achieve similar accuracy while the AC ensemble method can save more than 90% of the computational time.

TABLE 10 Errors $\|\phi_{J_0} - \phi_h\|_0 + \|u_{J_0} - u_h\|_0$ and CPU elapsed time for AC ensemble and NIDDM.

	$NIDDM$	$CPU\ time\ for\ NIDDM$	$Ensemble_{AC}$	$CPU\ time\ for\ AC\ ensemble$
$\Delta t = 1/20$	5.9903×10^{-2}	3.3866×10^{4}	7.5587×10^{-2}	3212
$\Delta t = 1/40$	3.0254×10^{-2}	4.9886×10^{4}	3.4202×10^{-2}	4495
$\Delta t = 1/80$	1.5951×10^{-2}	8.3646×10^{4}	1.6286×10^{-2}	6711
$\Delta t = 1/160$	8.1887×10^{-3}	1.5210×10^{5}	8.1843×10^{-3}	9137
$\Delta t = 1/320$	4.3874×10^{-3}	3.1790×10^{5}	3.8973×10^{-3}	12308

Furthermore, we also test more realistic hydraulic conductivity parameter k which is chosen as a uniformly distributed random number in $[10^{-6}, 2\times10^{-6}]$. In Table 11, NIDDM and the AC ensemble method achieve similar accuracy while the AC ensemble method can save more than 90% of the computational time.

TABLE 11 Errors $\|\phi_{J_0} - \phi_h\|_0 + \|u_{J_0} - u_h\|_0$ and CPU elapsed time for AC ensemble and NIDDM.

	$NIDDM$	$CPU\ time\ for\ NIDDM$	$Ensemble_{AC}$	$CPU\ time\ for\ AC\ ensemble$
$\Delta t = 1/20$	2.6302×10^{-2}	3.6490×10^{4}	2.8021×10^{-2}	3312
$\Delta t = 1/40$	1.3217×10^{-2}	5.5332×10^{4}	1.4152×10^{-2}	4456
$\Delta t = 1/80$	6.2938×10^{-3}	9.0661×10^{4}	7.0408×10^{-3}	6801
$\Delta t = 1/160$	3.2442×10^{-3}	1.5439×10^{5}	3.2311×10^{-3}	9231
$\Delta t = 1/320$	1.5448×10^{-3}	3.1934×10^{5}	1.5386×10^{-3}	12401

5.3 | Applicational simulation

Next, we apply our AC ensemble algorithm to a simplified simulation of the subsurface flow in a karst aquifer. As shown in Fig. 3, the computational domain is a unit square divided into the porous media domain D_p and the free flow domain D_f. Let D_f be the polygon $\overline{ABCDEFGHIJ}$ where $A = (0,1), B = (0,3/4), C = (1/2,1/4), D = (1/2,0), E = (3/4,0), F = (3/4,1/4), G = (1,1/4), H = (1,1/2), I = (3/4,1/2)$ and $J = (1/4,1)$. Let $D_p = \Omega/D_f$, $S_0 = \overline{AB} \cup \overline{JA}$, $S_1 = \overline{DE}$, and $S_2 = \overline{GH}$.

Set $T = 1$, $\alpha = 1$, $\nu = 1$, $g = 1$, $z = 0$. The boundary condition data and source terms are chosen to be 0 and let

$$u = \begin{cases} (U_0, 0)^T on & S_0 \\ (0, U_1)^T on & S_1 \\ (U_3, 0)^T on & S_2 \end{cases}$$

where U_i are constants. We subdivide Ω into rectangle of height and width $h = 1/M$, where M denotes a positive integer, and then subdivide each rectangle into two triangles by drawing a diagonal. For this numerical experiment, we choose $M = 32$ and $\triangle t = h$. In the following, we will provide the numerical results at $T = 1$ for the algorithm. We construct the random hydraulic conductivity tensor as follows

$$k(\vec{x},\omega) = a_0 + exp\left\{ \left[Y_1(\omega)cos(\pi y) + Y_3(\omega)sin(\pi y)\right] e^{-\frac{1}{8}} + \left[Y_2(\omega)cos(\pi x) + Y_4(\omega)sin(\pi x)\right] e^{-\frac{1}{8}} \right\}.$$

where $\vec{x} = (x,y)^T$, $a_0 = 1/100$, and $Y_1, \ldots, Y_4$ are independent and identically distributed with zero mean and unit variance.

Figure 4 shows some realizations of the logarithm of the hydraulic conductivity coefficient. In the first test, we set $U_1 = U_2 = -1$ and $U_0 = 2$ so that the total inflow rate is equal to the total outflow rate. In the second test, we keep the same U_1 and U_2 but set $U_0 = 1$ so that the total inflow rate is larger than the total outflow rate. This causes more water to be pushed out of the conduits into the porous media, which happens during a rain season. In the third test, we keep the same U_1 and U_2 but set $U_0 = 3$

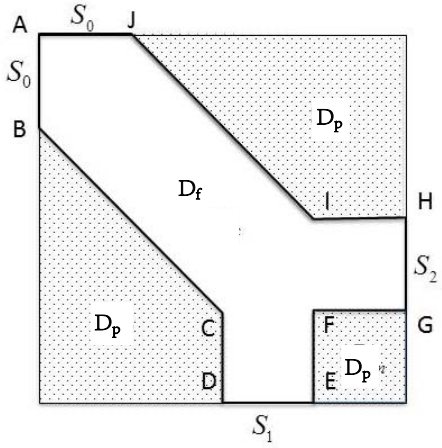

FIGURE 3 An illustration of the problem domain for the numerical experiment.

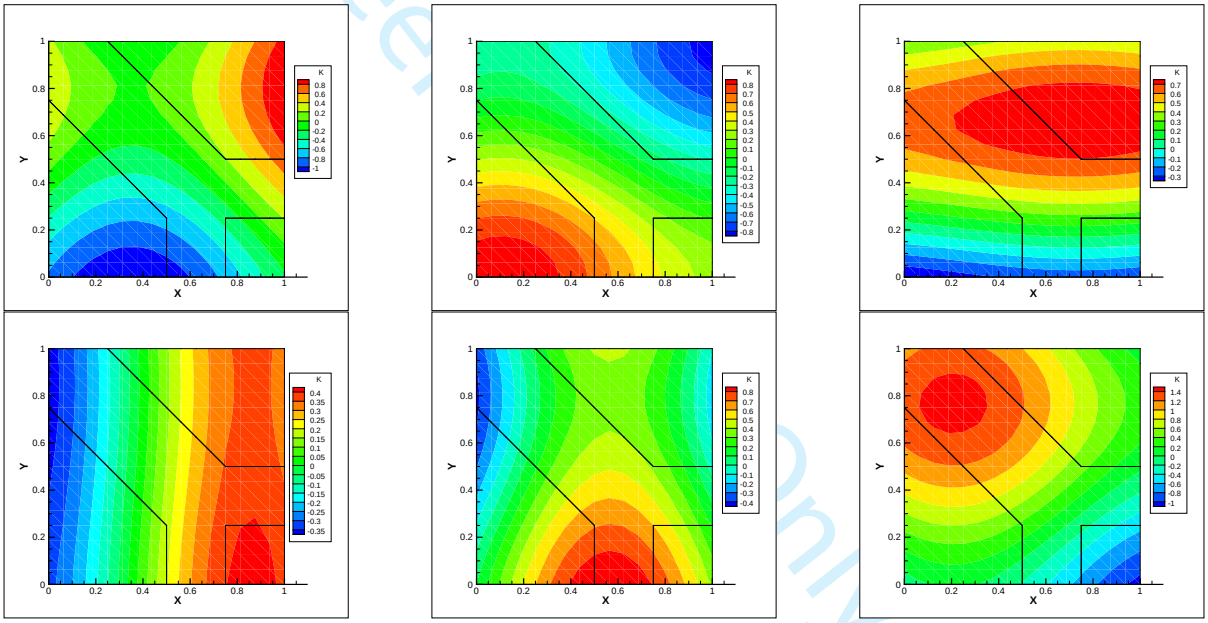

FIGURE 4 some realizations of log(k)

so that the total inflow rate is smaller than the total outflow rate. The more outflow causes more water to flow into the conduits from the porous media, which is what happens during a dry season. The three graphs in Figure 5 and Figure 7 illustrate the mean and variance of numerical solutions at the end time $T = 1$ for these three tests. These phenomena are expected due to the chosen unbalanced inflow and outflow rates for the conduit. Compared to the solutions of the traditional method (Figure 6 and Figure 8), we can find they have the same general behavior of the flow while our AC ensemble algorithm is much more efficient. Furthermore, the proposed method also works well for the realistic parameter values with $k = 10^{-4}, 10^{-6}$, and 10^{-8}, see Figure 9. In Figure 10, the graphs show energy $E = \|u_h\|_0^2 + \|\phi_h\|_0^2$ versus t. We can find there is an upward fluctuation in the graph with $\Delta t = 1/5$ and other graphs with smaller time steps become relatively stable, which is consistent with our theoretical result that a time-step condition must be satisfied to ensure stability and convergence. Moreover, when $k = 10^{-6}$ and $k = 10^{-8}$, we can find the results will have minor fluctuation for $\Delta t = 1/10$, and then they will become stable as the smaller time-step conditions.

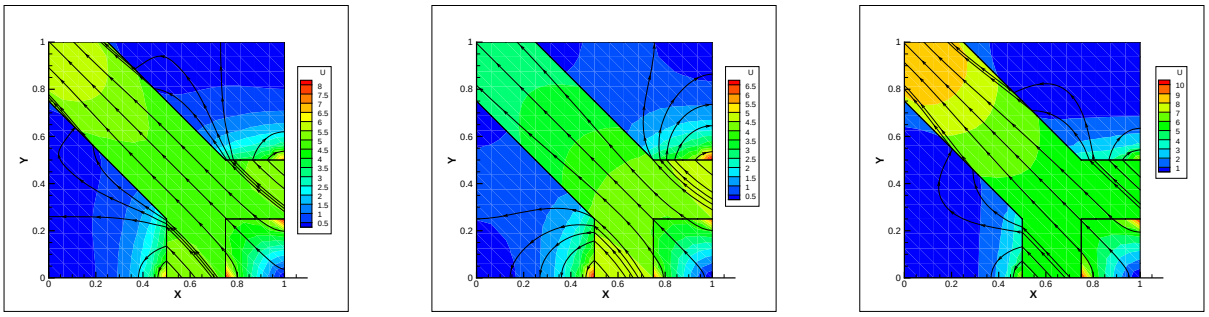

FIGURE 5 Plots of the ensemble mean for the ensemble AC method for $U_1 = -1$, $U_2 = -1$, and different U_0: $U_0 = 2$ in the left graph, $U_0 = 1$ in the middle graph, and $U_0 = 3$ in the right graph.

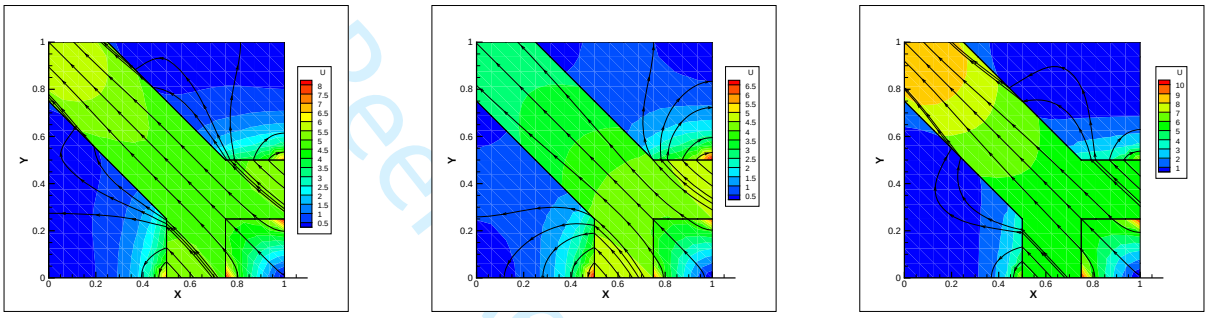

FIGURE 6 Plots of the ensemble mean for the traditional method for $U_1 = -1$, $U_2 = -1$, and different U_0: $U_0 = 2$ in the left graph, $U_0 = 1$ in the middle graph, and $U_0 = 3$ in the right graph.

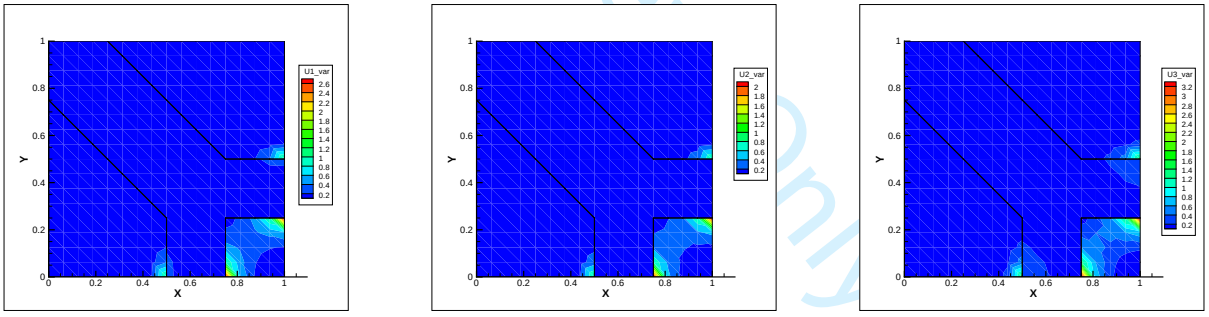

FIGURE 7 Plot of the variance of the ensemble AC method for $Q_1 = -1$, $Q_2 = -1$, and different Q_0: $Q_0 = 2$ in the left graph, $Q_0 = 1$ in the middle graph, and $Q_0 = 3$ in the right graph.

At last, we consider the more realistic case where the hydraulic conductivity tensor is non-diagonal, for which we need to use Algorithm 1 for ensemble computation. Let

$$\mathcal{K}(\vec{x},\omega) = \begin{bmatrix} k_{11}(\vec{x},\omega) & k_{12}(\vec{x},\omega) \\ k_{21}(\vec{x},\omega) & k_{22}(\vec{x},\omega) \end{bmatrix},$$

where $k_{11}(\vec{x},\omega) = k_{22}(\vec{x},\omega) \neq 0$ and $k_{21}(\vec{x},\omega) = k_{12}(\vec{x},\omega) \neq 0$, i.e. $\mathcal{K}(\vec{x},\omega)$ is not diagonal but symmetric.

$$k_{11}(\vec{x},\omega) = k_{22}(\vec{x},\omega) = a_1 + \sigma\sqrt{\lambda_0}Y_0(\omega) + \sum_{i=1}^{n_f} \sigma\sqrt{\lambda_i}[Y_i(\omega)cos(i\pi y) + Y_{n_f+i}(\omega)sin(i\pi y)],$$

$$k_{21}(\vec{x},\omega) = k_{12}(\vec{x},\omega) = a_2 + \sigma\sqrt{\lambda_0}Y_0(\omega) + \sum_{i=1}^{n_f} \sigma\sqrt{\lambda_i}[Y_i(\omega)cos(i\pi y) + Y_{n_f+i}(\omega)sin(i\pi y)].$$

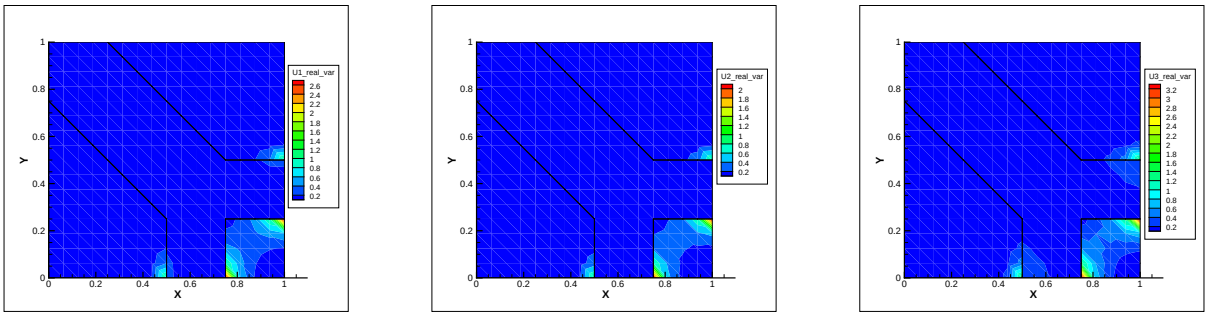

FIGURE 8 Plot of the variance of the traditional method for $Q_1 = -1$, $Q_2 = -1$, and different Q_0: $Q_0 = 2$ in the left graph, $Q_0 = 1$ in the middle graph, and $Q_0 = 3$ in the right graph.

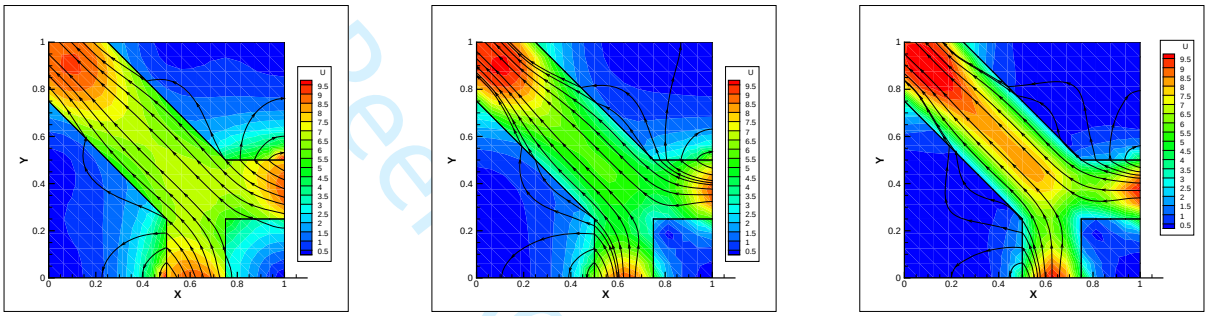

FIGURE 9 Plots of the ensemble mean for the ensemble AC method with $k = 10^{-4}, 10^{-6}$, and 10^{-8} (left, middle, right) for $U_1 = -2$, $U_2 = -2$, and $U_0 = 3$.

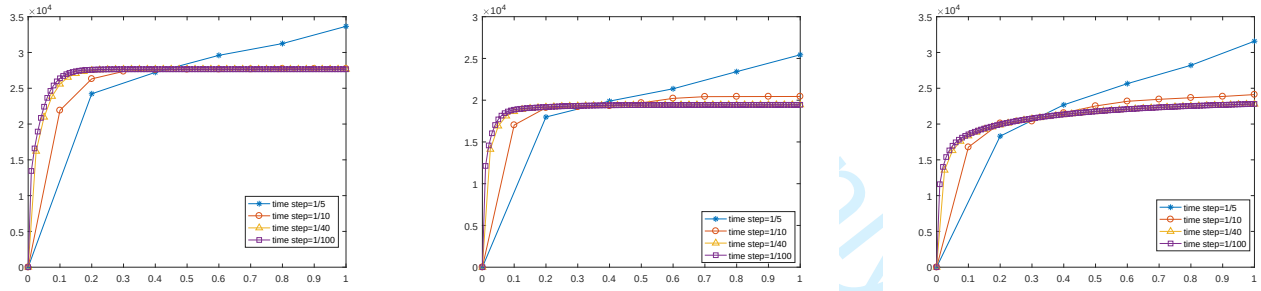

FIGURE 10 Plots of the ensemble mean for the ensemble AC method with $k = 10^{-4}, 10^{-6}$, and 10^{-8} (left, middle, right) for $U_1 = -2$, $U_2 = -2$, and $U_0 = 3$ as well as different time steps.

We take $a_1 = 10$ and $a_2 = 1$ such that the random hydraulic conductivity tensor $\mathcal{K}(\vec{x}, \omega)$ is SPD. The corresponding forcing term for the Darcy equation is $f_p = (1 + k_{11}(\vec{x}, \omega) - k_{22}(\vec{x}, \omega))(e^y - e^{-y})sin(x)e^t - (k_{12}(\vec{x}, \omega) + k_{21}(\vec{x}, \omega))(e^y - e^{-y})cos(x)e^t$; for the Stokes equations, f_{f_1} and f_{f_2} are the same as those in Section 5.2. The boundary conditions and initial conditions are also the same as those in Section 5.2.

We consider a group of simulations with $J = 100$ using the Monte Carlo method for sampling. Figure 11 shows the numerical results of our ensemble algorithm (Algorithm 1) and those of individual runs for comparison. The speed contours and velocity streamlines of the ensemble mean are computed for both approaches at $T = 0.5$ with $J = 100$ realizations, and then presented in Figure 11. It can be seen that both approaches capture the same general behavior of the flow while our AC ensemble algorithm is much more efficient.

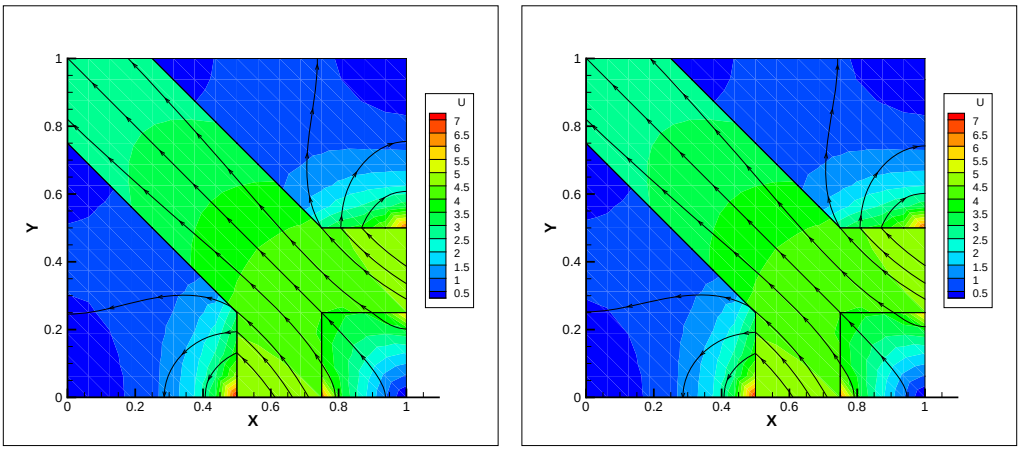

FIGURE 11 Speed contours and velocity streamlines for $U_0 = 1$, $U_1 = -1$, $U_2 = -1$, based on the ensemble mean obtained from our ensemble algorithm (left) and the traditional method (right) and with $J = 100$ at $T = 0.5$.

6 | CONCLUSIONS

Ensemble calculation is essential in uncertainty quantification, numerical weather prediction, sensitivity analysis and so on. The most efficient way to calculate such an ensemble will vary widely depending on the application, flow, computational resources and code used. In this article, an efficient, artificial compressibility ensemble algorithm is proposed for fast computation of the stochastic Stokes-Darcy systems. In this algorithm, the linear systems with two shared common coefficient matrices for all realizations at each time step can be solved by efficient iterative or direct methods at greatly reduced computational cost. Moreover, the fully coupled Stokes-Darcy system can be decoupled into two smaller sub-physics problems, which reduces the size of the linear systems to be solved and allows parallel computation of the two sub-physics problems. Furthermore, the velocity and pressure solves can be decoupled by the artificial compressibility method resulting in a simple updating step for the pressure. Therefore the storage requirements can be reduced and the computational speed is faster than traditional method and the ensemble method in[60]. The long time stability and first order accuracy in time under a time-step condition and two parameter conditions are proved for this algorithm. Furthermore, we also present an alternative algorithm for the case that the hydraulic conductivity tensor $\mathcal{K}$ is diagonal. This algorithm is long time stable under a time-step condition, *without* any parameter conditions. By the numerical experiments, we show the algorithm is also first order convergent in time, illustrate how to incorporate the artificial compressibility ensemble algorithm with the Monte Carlo method, and demonstrate the efficiency and effectiveness of this ensemble algorithm. We also apply the artificial compressibility ensemble algorithm to a simulation of the subsurface flow in a karst aquifer and discuss the phenomena of different unbalanced inflow and outflow rates for the conduit.

References

1. Arbogast T, Lehr HL. Homogenization of a Darcy-Stokes system modeling vuggy porous media. *Comput. Geosci.* 2006; 10(3): 291-302.

2. Çeşmelioğlu A, Rivière B. Primal discontinuous Galerkin methods for time-dependent coupled surface and subsurface flow. *J. Sci. Comput.* 2009; 40(1-3): 115-140.

3. Discacciati M. *Domain decomposition methods for the coupling of surface and groundwater flows*. PhD thesis. Ecole Polytechnique Fédérale de Lausanne, Switzerland; 2004.

4. Ervin VJ, Jenkins EW, Sun S. Coupled generalized nonlinear Stokes flow with flow through a porous medium. *SIAM J. Numer. Anal.* 2009; 47(2): 929-952.

5. Hanspal N, Waghode A, Nassehi V, Wakeman R. Numerical analysis of coupled Stokes/Darcy flow in industrial filtrations. *Transp. Porous Media* 2006; 64: 73-101.

6. He XM, Li J, Lin Y, Ming J. A domain decomposition method for the steady-state Navier-Stokes-Darcy model with Beavers-Joseph interface condition. *SIAM J. Sci. Comput.* 2015; 37(5): S264-S290.

7. Hoppe R, Porta P, Vassilevski Y. Computational issues related to iterative coupling of subsurface and channel flows. *Calcolo* 2007; 44(1): 1-20.

8. Layton W, Tran H, Trenchea C. Analysis of long time stability and errors of two partitioned methods for uncoupling evolutionary groundwater-surface water flows. *SIAM J. Numer. Anal.* 2013; 51(1): 248-272.

9. Cao Y, Gunzburger M, Hua F, Wang X. Coupled Stokes-Darcy model with Beavers-Joseph interface boundary condition. *Comm. Math. Sci.* 2010; 8(1): 1-25.

10. Gao Y, He XM, Mei L, Yang X. Decoupled, linear, and energy stable finite element method for the Cahn-Hilliard-Navier-Stokes-Darcy phase field model. *SIAM J. Sci. Comput.* 2018; 40(1): B110-B137.

11. Han D, Sun D, Wang X. Two-phase flows in karstic geometry. *Math. Methods Appl. Sci.* 2014; 37(18): 3048-3063.

12. Boubendir Y, Tlupova S. Domain decomposition methods for solving Stokes-Darcy problems with boundary integrals. *SIAM J. Sci. Comput.* 2013; 35(1): B82-B106.

13. Cao Y, Gunzburger M, He XM, Wang X. Robin-Robin domain decomposition methods for the steady Stokes-Darcy model with Beaver-Joseph interface condition. *Numer. Math.* 2011; 117(4): 601-629.

14. Cao Y, Gunzburger M, He XM, Wang X. Parallel, non-iterative, multi-physics domain decomposition methods for time-dependent Stokes-Darcy systems. *Math. Comp.* 2014; 83(288): 1617-1644.

15. Chidyagwai P, Rivière B. On the solution of the coupled Navier-Stokes and Darcy equations. *Comput. Methods Appl. Mech. Engrg.* 2009; 198(47-48): 3806-3820.

16. Discacciati M, Quarteroni A, Valli A. Robin-Robin domain decomposition methods for the Stokes-Darcy coupling. *SIAM J. Numer. Anal.* 2007; 45(3): 1246-1268.

17. Discacciati M, Miglio E, Quarteroni A. Mathematical and numerical models for coupling surface and groundwater flows. *Appl. Numer. Math.* 2002; 43(1-2): 57-74.

18. Ervin VJ, Jenkins EW, Lee H. Approximation of the Stokes-Darcy system by optimization. *J. Sci. Comput.* 2014; 59(3): 775-794.

19. Galvis J, Sarkis M. Non-matching mortar discretization analysis for the coupling Stokes-Darcy equations. *Electron. Trans. Numer. Anal.* 2007; 26: 350-384.

20. Gatica GN, Oyarzúa R, Sayas FJ. A residual-based a posteriori error estimator for a fully-mixed formulation of the Stokes-Darcy coupled problem. *Comput. Methods Appl. Mech. Engrg.* 2011; 200(21-22): 1877-1891.

21. Girault V, Rivière B. DG approximation of coupled Navier-Stokes and Darcy equations by Beaver-Joseph-Saffman interface condition. *SIAM J. Numer. Anal* 2009; 47(3): 2052-2089.

22. Gunzburger M, He XM, Li B. On Ritz projection and multi-step backward differentiation schemes in decoupling the Stokes-Darcy model. *SIAM J. Numer. Anal.* 2018; 56(1): 397-427.

23. Hou J, He XM, Guo C, Wei M, Bai B. A dual-porosity-Stokes model and finite element method for coupling dual-porosity flow and free flow. *SIAM J. Sci. Comput.* 2016; 38(5): B710-B739.

24. Kanschat G, Riviére B. A strongly conservative finite element method for the coupling of Stokes and Darcy flow. *J. Comput. Phys.* 2010; 229: 5933-5943.

25. Layton WJ, Schieweck F, Yotov I. Coupling fluid flow with porous media flow. *SIAM J. Numer. Anal.* 2002; 40(6): 2195-2218.

26. Mu M, Xu J. A two-grid method of a mixed Stokes-Darcy model for coupling fluid flow with porous media flow. *SIAM J. Numer. Anal.* 2007; 45(5): 1801-1813.

27. Tlupova S, Cortez R. Boundary integral solutions of coupled Stokes and Darcy flows. *J. Comput. Phys.* 2009; 228(1): 158-179.

28. Girault V, Vassilev D, Yotov I. Mortar multiscale finite element methods for Stokes-Darcy flows. *Numer. Math.* 2014; 127(1): 93-165.

29. Wang W, Xu C. Spectral methods based on new formulations for coupled Stokes and Darcy equations. *J. Comput. Phys.* 2014; 257, part A: 126-142.

30. Beavers G, Joseph D. Boundary Conditions at a Naturally Impermeable Wall. *J. Fluid Mech.* 1967; 30: 197-207.

31. Saffman P. On the boundary condition at the interface of a porous medium. *Stud. Appl. Math.* 1971; 1: 93-101.

32. Jager W, Mikelic A. On the Boundary Condition at the Interface Between a Porous Medium and a Free Fluid. *SIAM J. Appl. Math.* 2000; 60: 1111-1127.

33. Xu X, Graham-Brady L. Computational stochastic homogenization of random media elliptic problems using Fourier Galerkin method. *Finite Elem. Anal. Des.* 2006; 42(7): 613-622.

34. Matthies H, Keese A. Galerkin methods for linear and nonlinear elliptic stochastic partial differential equations. *Comput. Methods Appl. Mech. Eng.* 2005; 194: 1295-1331.

35. Babuška I, Nobile F, Tempone R. A Stochastic Collocation Method for Elliptic Partial Differential Equations with Random Input Data. *SIAM J. Numer. Anal.* 2007; 45(3): 1005-1034.

36. Xiu D, Hesthaven J. High-order collocation methods for differential equations with random inputs. *SIAM J. Sci. Comput* 2005; 27: 1118-1139.

37. Benjamin G, Hector K, Mary FW, Tim W, Ivan Y, Dongxiao Z. Stochastic collocation and mixed finite elements for flow in porous media. *Comput. Meth. Appl. Mech. Engrg.* 2008; 197(43-44): 3547-3559.

38. Nobile F, Tempone R, Webster CG. A sparse grid stochastic collocation method for partial differential equations with random input data. *SIAM J. Numer. Anal.* 2008; 46: 2309-2345.

39. Hosder S, Walters R, Perez R. A non-intrusive polynomial chaos method for uncertainty propagation in CFD simulations, AIAA-Paper 2006-891. *44th AIAA Aerospace Sciences Meeting and Exhibit.* 2006.

40. Reagan M, Najm H, Ghanem R, Knio O. Uncertainty quantification in reacting-flow simulations through non-intrusive spectral projection. *Combustion and Flame.* 2003; 132: 545-555.

41. Barth A, Lang A. Multilevel Monte Carlo method with applications to stochastic partial differential equations. *Int. J. Appl. Comput. Math.* 2012; 89: 2479-2498.

42. Kuo F, Schwab C, Sloan I. Quasi-Monte Carlo finite element methods for a class of elliptic partial differential equations with random coefficients. *SIAM J. Numer. Anal.* 2012; 50: 3351-3374.

43. Helton J, Davis F. Latin hypercube sampling and the propagation of uncertainty in analyses of complex systems. *Reliability Engineering and System Safety.* 2003; 81: 23-69.

44. Burkardt J, Gunzburger M, Peterson J, Romero V. Comparison of pure and "Latinized" centroidal Voronoi tessellation against various other statistical sampling methods. *Reliability Engineering and System Safety* 2006; 91: 1266-1280.

45. Jiang N, Layton W. An algorithm for fast calculation of flow ensembles. *Int. J. Uncertain. Quantif.* 2014; 4: 273-301.

46. Gallopulos E, Simoncini V. Convergence of BLOCK GMRES and matrix polynomials. *Lin. Alg. Appl.* 1996; 247: 97-119.

47. Feng Y, Owen D, Peric D. A block Conjugate Gradient method applied to linear systems with multiple right hand sides. *Comp. Meth. Appl. Mech.* 1995; 127: 1-4.

48. Jiang N, Layton W. Numerical analysis of two ensemble eddy viscosity numerical regularizations of fluid motion. *Numer. Methods Partial Differential Eq.* 2015; 31: 630-651.

49. Jiang N. A higher order ensemble simulation algorithm for fluid flows. *J. Sci. Comput.* 2015; 64: 264-288.

50. Jiang N, Kaya S, Layton W. Analysis of model variance for ensemble based turbulence modeling. *Comput. Appl. Math.* 2015; 15: 173-188.

51. Gunzburger M, Jiang N, Schneier M. An ensemble-proper orthogonal decomposition method for the nonstationary Navier-Stokes equations. *SIAM J. Numer. Anal.* 2017; 55(1): 286-304.

52. Gunzburger M, Jiang N, Schneier M. A higher-order ensemble/proper orthogonal decomposition method for the nonstationary Navier-Stokes equations. *Int. J. Numer. Anal. Model.* 2018; 15: 608-627.

53. Jiang N. A second-order ensemble method based on a blended backward differentiation formula timestepping scheme for time-dependent Navier-Stokes equations. *Numer. Methods Partial Differential Eq.* 2017; 33: 34-61.

54. Jiang N, Schneier M. An efficient, partitioned ensemble algorithm for simulating ensembles of evolutionary MHD flows at low magnetic Reynolds number. *Numer. Methods Partial Differential Eq.* 2018; 34: 2129-2152.

55. Mohebujjaman M, Rebholz L. An efficient algorithm for computation of MHD flow ensembles. *Comput. Appl. Math.* 2017; 17: 121-137.

56. Gunzburger M, Jiang N, Wang Z. An efficient algorithm for simulating ensembles of parameterized flow problems. *IMA J. Numer. Anal.* 2019; 39: 1180-1205.

57. Gunzburger M, Jiang N, Wang Z. A second-order time-stepping scheme for simulating ensembles of parameterized flow problems. *Comput. Appl. Math.* 2019; 19: 681-701.

58. Fiordilino J. A second order ensemble timestepping algorithm for natural convection. *SIAM J. Numer. Anal.* 2018; 56: 816-837.

59. Jiang N. A pressure-correction ensemble scheme for computing evolutionary Boussinesq equations. *Journal of Scientific Computing* 2019; 80: 315-350.

60. Jiang N, Qiu C. An efficient ensemble algorithm for numerical approximation of stochastic Stokes-Darcy equations. *Comput. Methods Appl. Mech. Engrg.* 2019; 343: 249-275.

61. Chorin AJ. A numerical method for solving incompressible viscous flow problems. *J. Comput. Phys* 1967; 2: 12.

62. Temam R. Une méthode d'approximation de la solution des équations de Navier-Stokes. *Bull. Soc. Math. France.* 1968; 96: 115-152.

63. Temam R. Sur l'approximation de la solution des équations de Navier-Stokes par la méthode des pas fractionnaires. I. *Arch. Ration. Mech. Anal.* 1969; 32: 135-153.

64. Temam R. Sur l'approximation de la solution des équations de Navier-Stokes par la méthode des pas fractionnaires. II. *Arch. Ration. Mech. Anal.* 1969; 32: 377-385.

65. Kuznetsov B, Vladimirova N, Yanenko N. *Numerical calculation of the symmetrical flow of viscous incompressible liquid around a plate (in Russian).* Studies in Mathematics and its ApplicationsMoscow: Nauka . 1966.

66. Guermond J, Minev P. High-order time stepping for the incompressible Navier-Stokes equations. *SIAM J. Sci. Comput.* 2015; 37(6): A2656-A2681.

67. DeCaria V, Layton W, McLaughlin M. A conservative, second order, unconditionally stable artificial compression method. *Comput. Methods Appl. Mech. Engrg.* 2017; 325: 733-747.

68. Philippe A, Pierre F. Convergence results for the vector penalty-projection and two-step artificial compressibility methods. *Discrete Contin. Dyn. Syst. Ser. B* 2012; 17: 1383-1405.

69. Shen J. On error estimates of the penalty method for unsteady Navier-Stokes equations. *SIAM J. Numer. Anal.* 1995; 32: 386-403.

70. Shen J. On a new pseudocompressibility method for the incompressible Navier-Stokes equations. *Appl. Numer. Math.* 1996; 21: 71-90.

71. Girault V, Raviart P. Finite Element Methods for Navier-Stokes equations. *Springer-Verlag, New York-Heidelberg-Berlin* 1986.

72. Gunzburger M. Finite Element Methods for Viscous Incompressible Flows-A Guide to Theory, Practices, and Algorithms. *Academic Press.* 1989.

APPENDIX

A .LONG TIME STABILITY OF AN ALTERNATIVE ALGORITHM

Theorem 3 (Long time stability of Algorithm 2)**.** If there exist $\alpha_1, \alpha_2, \beta_1, \beta_2$ in (0, 1) such that the time-step condition (24) holds, then the Algorithm 2 is long time stable: for any $N > 0$,

$$\begin{aligned}
&\frac{1}{2}\|u_j^N\|_f^2 + \frac{gS_0}{2}\|\phi_j^N\|_p^2 + \Delta t^2\frac{C_2}{\beta_1^2}\|\nabla u_j^N\|_f^2 + \frac{\Delta t}{2\gamma}\|p_j^N\|_f^2 + \Delta t\sum_i \frac{\eta_i^{max}}{2}\int_I (u_j^N\cdot\hat{\tau}_i)^2\,ds \\
&+\left(\Delta t^2\frac{1}{gS_0}\frac{C_1}{\alpha_1^2} + \Delta t\frac{g(k_{max}-k_{min})}{2}\right)\|\nabla\phi_j^N\|_p^2 + \frac{\Delta t}{2\gamma}\sum_{n=0}^{N-1}\|p_j^{n+1}-p_j^n\|_f^2 \\
&\le \frac{1}{2}\|u_j^0\|_f^2 + \frac{gS_0}{2}\|\phi_j^0\|_p^2 + \Delta t^2\frac{C_2}{\beta_1^2}\|\nabla u_j^0\|_f^2 + \frac{\Delta t}{2\gamma}\|p_j^0\|_f^2 + \Delta t\sum_i \frac{\eta_i^{max}}{2}\int_I (u_j^0\cdot\hat{\tau}_i)^2\,ds \\
&+\left(\Delta t^2\frac{1}{gS_0}\frac{C_1}{\alpha_1^2} + \Delta t\frac{g(k_{max}-k_{min})}{2}\right)\|\nabla\phi_j^0\|_p^2 + \Delta t\sum_{n=0}^{N-1}\frac{C_{P,f}^2}{4\alpha_2\nu}\|f_{f,j}^{n+1}\|_f^2 + \Delta t\sum_{n=0}^{N-1}\frac{gC_{P,p}^2}{4\beta_2 k_{max}}\|f_{p,j}^{n+1}\|_p^2.
\end{aligned} \tag{A1}$$

Proof. Setting $v_h = u_j^{n+1}$, $\psi = \phi_j^{n+1}$ in Algorithm 2, replacing $\gamma\nabla\cdot u_j^{n+1}$ in the momentum equation by $p_j^{n+1}-p_j^n$, taking inner product of the mass conservation equation by $\gamma^{-1}p_j^{n+1}$ and adding all three equations yields

$$\begin{aligned}
&\frac{1}{2\Delta t}\|u_j^{n+1}\|_f^2 - \frac{1}{2\Delta t}\|u_j^n\|_f^2 + \frac{1}{2\Delta t}\|u_j^{n+1}-u_j^n\|_f^2 + \nu\|\nabla u_j^{n+1}\|_f^2 + \sum_i\int_I \eta_i^{max}(u_j^{n+1}\cdot\hat{\tau}_i)(u_j^{n+1}\cdot\hat{\tau}_i)\,ds \\
&+\frac{1}{2\gamma}\left(\|p_j^{n+1}\|_f^2 - \|p_j^n\|_f^2 + \|p_j^{n+1}-p_j^n\|_f^2\right) + \frac{gS_0}{2\Delta t}\|\phi_j^{n+1}\|_p^2 - \frac{gS_0}{2\Delta t}\|\phi_j^n\|_p^2 \\
&+\frac{gS_0}{2\Delta t}\|\phi_j^{n+1}-\phi_j^n\|_p^2 + gk_{max}(\nabla\phi_j^{n+1},\nabla\phi_j^{n+1})_p + c_I(u_j^{n+1},\phi_j^n) - c_I(u_j^n,\phi_j^{n+1}) \\
&= (f_{f,j}^{n+1},u_j^{n+1})_f + g(f_{p,j}^{n+1},\phi_j^{n+1})_p - \sum_i\int_I(\eta_{i,j}-\eta_i^{max})(u_j^n\cdot\hat{\tau}_i)(u_j^{n+1}\cdot\hat{\tau}_i)\,ds \\
&\quad - g((\mathcal{K}_j - k_{max}\mathcal{I})\nabla\phi_j^n,\nabla\phi_j^{n+1})_p.
\end{aligned} \tag{A2}$$

Since $\mathcal{K}_j(x)$ and $k_{max}\mathcal{I}$ are both symmetric, we have $|\mathcal{K}_j(x) - k_{max}\mathcal{I}|_2 \le k_{max} - k_{min}$. The main difference from the proof of Theorem 1 is on the estimates of the following two terms.

$$-\sum_i\int_I(\eta_{i,j}-\eta_i^{max})(u_j^n\cdot\hat{\tau}_i)(u_j^{n+1}\cdot\hat{\tau}_i)\,ds \tag{A3}$$

$$\leq \sum_i \left[\frac{\eta_i^{max}}{2} \int_I (u_j^n \cdot \widehat{\tau}_i)^2 \, ds + \frac{\eta_i^{max}}{2} \int_I (u_j^{n+1} \cdot \widehat{\tau}_i)^2 \, ds \right],$$

and

$$-g\left((\mathcal{K}_j - k_{max}\mathcal{I})\nabla\phi_j^n, \nabla\phi_j^{n+1}\right)_p \leq \frac{g(k_{max}-k_{min})}{2}\|\nabla\phi_j^n\|_p^2 + \frac{g(k_{max}-k_{min})}{2}\|\nabla\phi_j^{n+1}\|_p^2. \tag{A4}$$

The estimates of other terms are similar to those in the proof of Theorem 1. Combining all estimates we then have the following inequality

$$\begin{aligned}
&\frac{1}{2\Delta t}\|u_j^{n+1}\|_f^2 - \frac{1}{2\Delta t}\|u_j^n\|_f^2 + \left(1-\alpha_1-\alpha_2-\Delta t\frac{2C_2}{\beta_1^2\nu}\right)\nu\|\nabla u_j^{n+1}\|_f^2 + \Delta t\frac{C_2}{\beta_1^2}\left(\|\nabla u_j^{n+1}\|_f^2 - \|\nabla u_j^n\|_f^2\right) \\
&+ \sum_i \frac{\eta_i^{max}}{2}\left[\int_I (u_j^{n+1}\cdot\widehat{\tau}_i)^2\,ds - \int_I (u_j^n\cdot\widehat{\tau}_i)^2\,ds\right] + \frac{1}{2\gamma}\left(\|p_j^{n+1}\|_f^2 - \|p_j^n\|_f^2 + \|p_j^{n+1}-p_j^n\|_f^2\right) \\
&+ \frac{gS_0}{2\Delta t}\|\phi_j^{n+1}\|_p^2 - \frac{gS_0}{2\Delta t}\|\phi_j^n\|_p^2 + (1-\beta_1-\beta_2-\Delta t\frac{1}{g_0^2 k_{max}}\frac{2C_1}{\alpha_1^2} - \frac{k_{max}-k_{min}}{k_{max}})gk_{max}\|\nabla\phi_j^{n+1}\|_p^2 \\
&+ \left(\Delta t\frac{1}{gS_0}\frac{C_1}{\alpha_1^2} + \frac{g(k_{max}-k_{min})}{2}\right)\left(\|\nabla\phi_j^{n+1}\|_p^2 - \|\nabla\phi_j^n\|_p^2\right) \leq \frac{C_{P,f}^2}{4\alpha_2\nu}\|f_{f,j}^{n+1}\|_f^2 + \frac{gC_{P,p}^2}{4\beta_2 k_{max}}\|f_{p,j}^{n+1}\|_p^2.
\end{aligned} \tag{A5}$$

Since we assume $\mathcal{K}_j$ is SPD, and any two ensemble members have different hydraulic conductivity tensor $\mathcal{K}$, we have $k_{max} > k_{min} > 0$ and thus $0 < \frac{k_{max}-k_{min}}{k_{max}} < 1$. Thus no constraints on the parameters are required. Now if the time-step condition (24) holds, (A5) reduces to

$$\begin{aligned}
&\frac{1}{2\Delta t}\|u_j^{n+1}\|_f^2 - \frac{1}{2\Delta t}\|u_j^n\|_f^2 + \Delta t\frac{C_2}{\beta_1^2}\left(\|\nabla u_j^{n+1}\|_f^2 - \|\nabla u_j^n\|_f^2\right) \\
&+ \sum_i \frac{\eta_i^{max}}{2}\left[\int_I (u_j^{n+1}\cdot\widehat{\tau}_i)^2\,ds - \int_I (u_j^n\cdot\widehat{\tau}_i)^2\,ds\right] + \frac{1}{2\gamma}\left(\|p_j^{n+1}\|_f^2 - \|p_j^n\|_f^2 + \|p_j^{n+1}-p_j^n\|_f^2\right) \\
&+ \frac{gS_0}{2\Delta t}\|\phi_j^{n+1}\|_p^2 - \frac{gS_0}{2\Delta t}\|\phi_j^n\|_p^2 + \left(\Delta t\frac{1}{gS_0}\frac{C_1}{\alpha_1^2} + \frac{g(k_{max}-k_{min})}{2}\right)\left(\|\nabla\phi_j^{n+1}\|_p^2 - \|\nabla\phi_j^n\|_p^2\right) \\
&\leq \frac{C_{P,f}^2}{4\alpha_2\nu}\|f_{f,j}^{n+1}\|_f^2 + \frac{gC_{P,p}^2}{4\beta_2 k_{max}}\|f_{p,j}^{n+1}\|_p^2.
\end{aligned} \tag{A6}$$

Summing up (A6) from $n = 0$ to $N-1$ and multiplying through by Δt yields (A1). □